Ion microprobe survey of the grain-scale oxygen isotope geochemistry of minerals in metamorphic rocks

John M. Ferry [a,*], Kouki Kitajima [b], Ariel Strickland [b], John W. Valley [b]

[a] *Department of Earth and Planetary Sciences, Johns Hopkins University, Baltimore, MD 21218, USA*
[b] *WiscSIMS, Department of Geoscience, University of Wisconsin, Madison, WI 53706, USA*

Abstract

The oxygen isotope compositions of calcite, diopside, dolomite, forsterite, garnet, K-feldspar, kyanite, plagioclase, quartz, and wollastonite were analyzed in suites of contact and regional metamorphic rocks using an ion microprobe. Spatial resolution was $\sim$10 μm. Precision, measured as the standard deviation of working standards averaged over the entire project, was 0.13–0.18‰ for three carbonate standards and 0.11–0.12‰ for two silicate standards. A total of 1176 analyses (excluding standards) were made of 73 minerals in 23 samples. Both intercrystalline and intracrystalline variability in $\delta^{18}O$ is greater in contact than in regional metamorphic rocks. Of 27 minerals analyzed in contact metamorphosed rocks, 70% exhibit statistically significant grain-to-grain variability in $\delta^{18}O$ over areas $\leqslant$1.41 cm^2 with the largest range in silicates and carbonates in a single sample of 7.4‰ (forsterite) and 10.6‰ (dolomite). Of 88 grains analyzed in two or more places in contact metamorphosed rocks, 32% exhibit statistically significant intracrystalline variability in $\delta^{18}O$ with the largest range in a single silicate and carbonate grain of 3.1‰ (forsterite) and 10.1‰ (dolomite). In contrast, 44% of 45 minerals in regional metamorphic rocks exhibit significant grain-to-grain variability in $\delta^{18}O$ over areas $\leqslant$1.17 cm^2 with the largest range in silicates and carbonates in a single sample of only 1.1‰ (plagioclase) and 0.9‰ (calcite). Only 6% of 144 grains analyzed in two or more places in regional metamorphic rocks exhibit significant intracrystalline variability in $\delta^{18}O$ with the largest range in a single silicate and carbonate grain of only 1.5‰ (diopside) and 0.7‰ (calcite). The difference in intercrystalline and intracrystalline variability in $\delta^{18}O$ between contact and region metamorphic rocks is explained by the longer duration and slower reaction rates of regional metamorphism rather than to differences in temperature. There is no significant difference in intercrystalline and intracrystalline variability in $\delta^{18}O$ in regional metamorphic rocks among samples from the biotite, garnet, and kyanite zones. Calcite inclusions in forsterite, and calcite and quartz inclusions in garnet either have $\delta^{18}O$ that is statistically indistinguishable from $\delta^{18}O$ of the same mineral occurring as nearby matrix grains or have statistically significant lower $\delta^{18}O$. No reversed isotope fractionations were measured between coexisting mineral pairs. Minerals in individual samples, however, exhibit a wide range in the degree to which they attained and preserve oxygen isotope fractionations consistent with metamorphic temperatures recorded by mineral equilibria. Processes that account for grain-scale departures from isotope exchange equilibrium include: (a) overstepping of prograde mineral reactions, (b) growth zoning in low-diffusivity minerals, (c) interaction of rocks with fluids at the peak of metamorphism and/or during cooling, (d) retrograde mineral reactions, and (e) closed-system isotope exchange between coexisting minerals during cooling. This study provides new information about (1) the degree to which a variety of textural changes experienced by rocks during metamorphism are associated with changes in $\delta^{18}O$, (2) oxygen isotope homogenization at the outcrop scale among contrasting lithologies, (3) changes in $\delta^{18}O$ with increasing grade of regional metamorphism, and (4) time scales of metamorphic process.

---

* Corresponding author. Tel.: +1 410 516 8121; fax: +1 410 516 7933.
 E-mail address: jferry@jhu.edu (J.M. Ferry).

1. INTRODUCTION

The newest generation of large-radius, multi-collector ion microprobes is capable of in situ measurements of the oxygen isotope composition ($\delta^{18}O$) of minerals at a spatial scale of ~10 μm with a typical analytical precision of 0.1–0.2‰ (1 standard deviation, SD; Kita et al., 2009; Valley and Kita, 2009). The instrumentation therefore offers the opportunity to routinely and precisely analyze the $\delta^{18}O$ of minerals at a scale smaller than the grain size of most metamorphic rocks while preserving their petrologic context. Only one study to date, however, has analyzed multiple coexisting minerals (Gordon et al., 2012). A wide variety of common mineral assemblages in more typical metamorphic rocks has not been analyzed in petrologic context, in part because of a lack of appropriate mineral standards.

The goal of this study was to address this neglect by measuring the in situ grain-scale $\delta^{18}O$ of ten different common minerals in suites of contact and Barrovian regional metamorphic rocks that include a range of lithologies and metamorphic grade. The primary aim of the research was to: (1) assess the grain-to-grain variability in $\delta^{18}O$ of each mineral in each sample, (2) evaluate whether individual mineral grains are homogeneous or zoned in $\delta^{18}O$ and the degree of variability, if zoned, and (3) determine the grain-scale oxygen isotope fractionation between each different coexisting mineral pair in each sample. In addition, in selected samples, we evaluated: (a) whether the $\delta^{18}O$ of a mineral differed between its occurrence in the matrix and as inclusions in another mineral, (b) the likely mechanisms that produced grain-to-grain variability and intracrystalline zoning of minerals in $\delta^{18}O$, (c) the effects of infiltration of low-$\delta^{18}O$ fluids during both contact and regional metamorphism, and (d) the degree to which variations in $\delta^{18}O$ can be correlated with a variety of grain-scale textural features.

2. GEOLOGICAL CONTEXT AND SCOPE OF STUDY

Table 1 summarizes the location, mineralogy, petrology, and geologic context of all analyzed samples.

2.1. Geological context of contact metamorphic rocks

Building on Ferry et al. (2010, 2011), additional analyses of dolomite, calcite, forsterite, and diopside were obtained from six samples of dolomite and siliceous dolomite marbles from the Ballachulish and Beinn an Dubhaich aureoles, Scotland, and from the Twin Lakes pendant, Sierra Nevada, California. In addition, quartz, calcite, K-feldspar, anorthite, diopside, wollastonite, and grossular garnet were analyzed in calc-silicate rocks, one each from the Twin Lakes and Mt. Morrison pendants, Sierra Nevada. All the principal minerals were analyzed in the samples of contact metamorphic rocks. Pressure (P) and temperature (T) of metamorphism are in the ranges 0.5–3.0 kbar and 560–735 °C. Four of the eight samples of contact metamorphic rocks were deliberately chosen from the Twin Lakes pen-

dant to assess oxygen isotope behavior in a range of rock types metamorphosed at the same P–T conditions.

2.2. Geological context of regional metamorphic rocks

Analysis of regional metamorphic rocks focused on fifteen samples from Barrovian terrains in eastern Vermont, USA, and the Central Swiss Alps. The most common metasedimentary protolith lithologies are represented: pelite (6 samples), psammite (3 samples), and marl (6 samples). With reference to index minerals in pelitic schists, the 15 samples are from the biotite zone (2), garnet zone (3), and kyanite zone (10). With three exceptions, where present, quartz, calcite, K-feldspar, plagioclase, kyanite, diopside, and garnet were analyzed in each sample. The exceptions are three samples for which data for only a single mineral are reported. Other principal minerals in the rocks, ankerite, muscovite, paragonite, biotite, chlorite, staurolite, and amphibole, were not analyzed because suitable standards had not been developed. In addition, amphibole and the sheet silicates may exhibit significant orientation effects, although this has been demonstrated only for oxides like magnetite, hematite, and rutile (Huberty et al., 2010). The P–T conditions of metamorphism are in the ranges 7–8 kbar and 475–635 °C. The T assigned to locations Q2A and 21-28A (Table 1) has been revised upward to 525 °C (midway between the values preferred by Ferry, 1994, for the garnet and kyanite zones) because some pelite samples from both locations contain staurolite. Ten of the 15 samples are from a single stratigraphic unit in east-central Vermont (Fig. 1) to evaluate the effects of lithology and grade on oxygen isotope behavior within the context of a single, well-studied occurrence of progressive regional metamorphism. Fig. 1 provides a convenient reference for relating sample numbers in the text, figures, and tables to the geological context of the ten samples.

2.3. Scope of study

Seventy-three different minerals were analyzed in the 23 samples. Normally 10–20 spot analyses were performed of each mineral in each sample to assess both grain-to-grain and intracrystalline variability in $\delta^{18}O$. The minimum number of analyses was six (plagioclase in sample Q2A), and the maximum number was 48 (quartz in sample 21-29G). The total number of individual measurements of $\delta^{18}O$, excluding standards, was 1141.

Data collected in this study were supplemented by 35 analyses from Ferry et al. (2010). These included 25 analyses of dolomite in samples B1W (10) and B43A (15) and ten analyses of forsterite in sample B1W. Generally, analyses from the current study are preferred because of the significantly improved precision that results from analysis of silicates with a garnet or quartz rather than a calcite working standard. Dolomite in samples B1W and B43A are uniform in $\delta^{18}O$, and additional analyses were not warranted. Analyses of forsterite from Ferry et al. (2010) are included because they exhibit the largest range in $\delta^{18}O$ of any analyzed silicate mineral in either study.

Table 1
Summary of geologic and petrologic information about samples investigated.

Sample[a]	Location	Age (Ma)	Lithology/Petrology	T (°C)	P (kbars)	Mineralogy[b]	Ref[c]
A. Contact metamorphic rocks							
B1W	Beinn an Dubhaich aureole, Scotland	54	Marble	690	0.5	Dol-Fo-Cal	1,2,3
B43A	Beinn an Dubhaich aureole, Scotland	54	Fo-Cal vein in Dol marble	655	0.5	Dol-Fo-Cal	1,2,3
CL30O	Mt. Morrison pendant, California, USA	~89	Hornfels, 1 m from Wo isograd	560	1.5	Qtz-Wo-Kfs-Di-Cal	4,5
G1A	Ballachulish aureole, Scotland	423	Marble	735	3.0	Cal-Fo-Dol	6,7,8
KP1B	Twin Lakes pendant, California, USA	80–100	Siliceous dolomitic marble	595	~1.8	Di-Cal-Fo-Dol	2,3,9
KP1K	Twin Lakes pendant, California, USA	80–100	Marble	595	~1.8	Dol	3,9
KP1L	Twin Lakes pendant, California, USA	80–100	Fo-Cal vein in Dol marble	595	~1.8	Dol-Fo-Cal	2,3,9
KP3E	Twin Lakes pendant, California, USA	80–100	Calc-silicate marble	595	~1.8	Cal-Wo-Di-Kfs-An-Grs-Qtz-Ttn	2,3,9

Sample[a]	Location	Age (Ma)	Lithology/Petrology	Zone[d]	T (°C)	P (kbars)	Mineralogy[b]	Ref[c]
B. Regional metamorphic rocks								
E6	Val d'Efra, Central Swiss Alps	~25	Pelitic schist	Ky	630	~7	Ms-Bt-Grt-St-Ky-Pl-Qtz	10,11
Gass	Gassetts, Vermont, USA	~380	Pelitic schist	Ky	540–635	~7–10	Ms-Pg-Bt-Grt-St-Ky-Qtz	12
Q1d	Gile Mountain Fm., east-central Vermont, USA	~355	Psammite	Bt	475	~7–8	Qtz-Bt-Ms-Pl-Cal-Ank	13,14,15,16
Q1J	Gile Mountain Fm., east-central Vermont, USA	~355	Marl	Bt	475	~7–8	Cal-Ank-Qtz-Ms-Pl	13,14,15,16
Q2A	Gile Mountain Fm., east-central Vermont, USA	~355	Pelitic schist	Grt-St	525	~7–8	Ms-Bt-Chl-Grt-Pl-Qtz	13,14,16
3-4F	Waits River Fm., southeast Vermont, USA	~366	Marl	Ky	575	~7–8	Cal-Di-Cam-Bt-Kfs-Pl-Czo-Qtz	17,18,19
3-4G	Waits River Fm., southeast Vermont, USA	~366	Marl	Ky	575	~7–8	Cal-Di-Cam-Bt-Kfs-Pl-Czo-Qtz	17,18,19
21-24C	Gile Mountain Fm., east-central Vermont, USA	~355	Marl	Ky	550	~7–8	Cal-Qtz-Bt-Ms-Chl-Grt-Pl	14,16
21-25C	Gile Mountain Fm., east-central Vermont, USA	~355	Psammite	Ky	550	~7–8	Qtz-Grt-Bt-Ms-Chl-Pl-Cal	14,16
21-25J	Gile Mountain Fm., east-central Vermont, USA	~355	Pelitic schist	Ky	550	~7–8	Bt-Ms-Pl-Czo-Qtz-Cal	14,16
21-26E	Gile Mountain Fm., east-central Vermont, USA	~355	Psammite	Grt	500	~7–8	Qtz-Grt-Bt-Ms-Pl-Cal	2,14,16
21-28A	Gile Mountain Fm., east-central Vermont, USA	~355	Pelitic schist	Grt-St	525	~7–8	Ms-Pg-Bt-Chl-Grt-Pl-Qtz	14,16
21-29C	Gile Mountain Fm., east-central Vermont, USA	~355	Marl	Ky	550	~7–8	Cal-Ank-Grt-Cam-Bt-Ms-Chl-Pl-Czo-Qtz	14,16
21-29G	Gile Mountain Fm., east-central Vermont, USA	~355	Pelitic schist	Ky	550	~7–8	Ms-Bt-Chl-Grt-Ky-Pl-Qtz	14,16
34-1A	Waits River Fm., central Vermont, USA	~368	Marl	Ky	575	~7–8	Cal-Di-Cam-Kfs-Pl-Czo-Qtz	17,18,19

[a] Sample locations in the Gile Mountain Formation in Fig. 1 are denoted by that part of the sample number that precedes the final letter.

[b] Mineral abbreviations: An = anorthite, Ank = ankerite, Bt = biotite, Cal = calcite, Cam = calcic amphibole, Chl = chlorite, Czo = clinozoisite, Di = diopside, Dol = dolomite, Fo = forsterite, Grs = grossular, Grt = garnet, Kfs = K-feldspar, Ky = kyanite, Ms = muscovite, Pg = paragonite, Pl = plagioclase, Qtz = quartz, St = staurolite, Ttn = titanite, Wo = wollastonite.

[c] References: 1 = Ferry and Rumble (1997), 2 = Ferry et al. (2010), 3 = Ferry et al. (2011), 4 = Ferry et al. (2001), 5 = Lackey and Valley (2004), 6 = Masch and Heuss-Aßbichler (1991), 7 = Ferry (1996a, 1996b), 8 = Fraser et al. (2004), 9 = Davis and Ferry (1993), 10 = Ferry et al. (2005), 11 = Rubatto et al. (2009), 12 = Vance and Holland (1993), 13 = Ferry (1988), 14 = Ferry (1994), 15 = Ferry (2007), 16 = Wing et al. (2003), 17 = Ferry (1992), 18 = Stern et al. (1992), 19 = Ratcliffe et al. (2001).

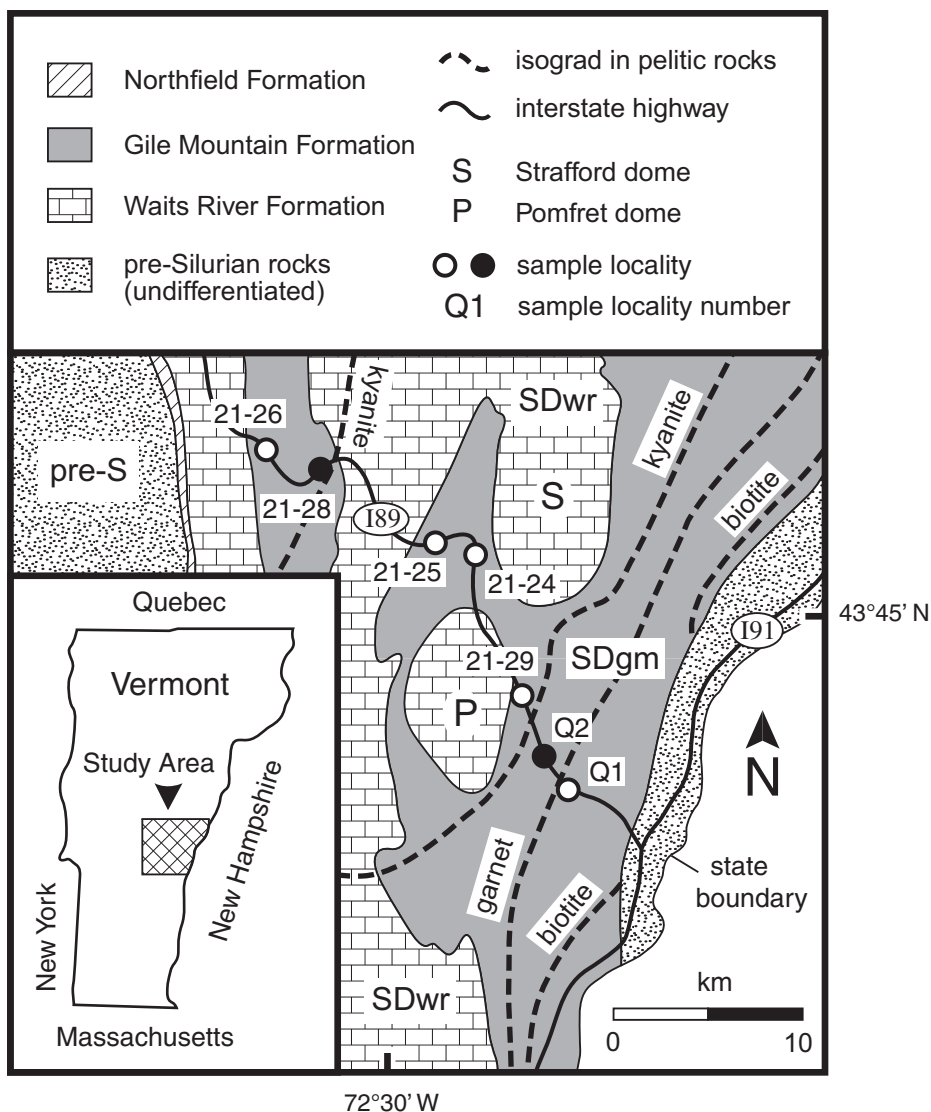[d] With respect to index minerals in pelitic schists.

Fig. 1. Geological sketch map (after Lyons, 1955; Doll et al., 1961) of the area in east-central Vermont where ten of fifteen analyzed samples of regional metamorphic rocks were collected from the Gile Mountain Formation. Sample location numbers are the same in this study as in Ferry (1988, 1994, 2007). Black circles identify locations in the Gile Mountain Formation where some pelites in the garnet zone contain staurolite. SDgm = Siluro-Devonian Gile Mountain Formation; SDwr = Siluro-Devonian Waits River Formation; pre-S = pre-Silurian units, undifferentiated.

3. METHODS OF INVESTIGATION

3.1. Sample sources

With one exception, all samples have been the subject of previous research by the authors (Table 1). Sample numbers used in the text, figures, and tables that follow are the same as in earlier publications. The exception is a sample of the Gassetts schist (Gass), an icon of New England geology that has been extensively studied by others (e.g., Vance and Holland, 1993, and references therein).

3.2. Sample mounts and preparation

Samples B1W, B43A, KP1B, KP1L, and KP3E are ~2.5-cm diameter, 5 mm thick circular disks used in a pre-

vious study (Ferry et al., 2010). UWG2 garnet standard (Valley et al., 1995) was newly mounted at the center of each disk as the working silicate standard and the disks were repolished. The other samples were 2.54-cm diameter circular polished thin sections. A thin section was also prepared of sample KP1L to image zones of turbid dolomite for $\delta^{18}O$ analysis that are invisible in the disk. UWG2 garnet standard was mounted as a working standard at the center of thin sections in which silicates were analyzed, and either a calcite or dolomite standard was mounted in sections in which carbonates were analyzed. The UWQ1 quartz standard (Kelly et al., 2007) was additionally mounted in samples 21-29C and 21-29G.

Polished, uncoated samples were examined in reflected and transmitted light and using back backscattered electron (BSE) imaging with the Hitachi S3400N variable pressure

scanning electron microscope in the Department of Geoscience at the University of Wisconsin. All samples were cleaned by multiple rinsings and sonication in ethanol and distilled water and coated with a ~30 nm layer of Au.

3.3. Ion microprobe analysis

In situ oxygen isotope analyses of carbonate and silicate minerals in all samples were obtained during three five-day and two one-day analytical sessions with the CAMECA ims-1280 ion microprobe in the WiscSIMS Laboratory, Department of Geoscience, at the University of Wisconsin, using operating and analytical conditions described in greater detail by Kita et al. (2009), Valley and Kita (2009), and Ferry et al. (2010). The primary ion beam was focused to ~10 μm on the sample surface. Ion currents were in the range 1.3–1.6 nA during analysis of carbonates and 1.8–2.1 nA during analysis of silicates. Analysis pit depths were ~1 μm. Analyses were normally performed at spots located within 7 mm of the center of the sample mount. The duration of each analysis was 3–4 min. The working standards were: UWC1 calcite and UWC3 calcite for analyses of calcite (and dolomite in sample KP1B), UW6220 dolomite for analyses of dolomite in samples KP1K and KP1L, UWQ1 for analyses of quartz in samples 21-29C and 21-29G, and UWG2 garnet for all other analyses of silicate minerals. The working standard in each sample was measured four times before and after usually every 10 unknown analyses (minimum every 5; maximum every 20). Over the entire project, the average (and range) of the standard deviation (SD) of the working standards were: UWC1, 0.14‰ (0.08–0.25‰); UWC3, 0.13‰ (0.09–0.21‰); UW6220, 0.18‰ (0.13–0.23‰); UWQ1, 0.11‰ (0.10–0.13‰); and UWG2, 0.12‰ (0.05–0.22‰). The raw $\delta^{18}O$ data for unknowns were corrected using established procedures at the WiscSIMS Laboratory (Ushikubo et al., 2012; Nakashima et al., 2013; Tenner et al., 2013). Corrections involved two terms. Following the notation of Tenner et al. (2013, their Electronic Annex 1), one term is *bias*(WS), computed just from the raw $\delta^{18}O$ of the working standard (WS) measured during analysis of the unknowns and the $\delta^{18}O$ of the working standard on the VSMOW scale. The second term is *bias**(*unknown*) that additionally corrects for any difference in chemical composition and crystal structure between each unknown mineral and the working standard (only used when such a difference exists). The *bias**(*unknown*) correction was calibrated (1) from at least four measurements of the raw $\delta^{18}O$ both of the working standard and, as appropriate, of one or more 29 additional mineral standards (made once during each analytical session) and (2) from $\delta^{18}O$ of the mineral standards on the VSMOW scale. Further information about corrections to the raw data is given in Appendix A along with the oxygen isotope compositions and relevant chemical data for all 30 standards.

3.4. Post-analysis examination and analysis of the samples

Following ion microprobe analysis, the Au coat was removed from each sample and replaced with a C coat.

Every ion microprobe analysis pit was examined by BSE imaging to verify that none were compromised by inclusions of other minerals, epoxy or other irregular features. The thin section of sample KP1L was examined by cathodoluminescence at the Ruhr-University Bochum, Germany, using instrumentation and methods described by Schertl et al. (2004). To make the *bias**(*unknown*) correction as accurately as possible, the chemical compositions of calcite, dolomite, garnet, and plagioclase adjacent to each ion microprobe analysis pit were measured. Chemical analyses were performed with the JEOL JXA-8600 electron microprobe at Johns Hopkins University using wavelength-dispersive spectrometry, natural and synthetic silicate and carbonate mineral standards, and a ZAF correction scheme (Armstrong, 1995).

4. RESULTS

All ion microprobe measurements of $\delta^{18}O$ of the standards and unknowns, selected instrument readings for each analysis, and relevant chemical data for calcite, dolomite, plagioclase, and garnet in all analyzed samples are compiled in Appendix B. A summary of results is given in Table 2.

4.1. Grain-to grain variability in oxygen isotope composition

4.1.1. Definition and assessment of homogeneity

A fundamental question addressed in this study is the degree to which minerals in metamorphic rocks are homogeneous or variable in $\delta^{18}O$ at the grain-size scale. The criterion for homogeneity follows Ferry et al. (2010). A given mineral in a given sample is considered homogeneous if all analyses of the mineral are statistically consistent with a single value at a 95% confidence level as judged by the mean square weighted deviate (MSWD), calculated following Mahon (1996). Otherwise, the mineral is considered not homogeneous. The MSWD statistic quantitatively accounts for differences both in the number of analyses made of a mineral in a sample and in the SD of the working standard during analysis. Homogeneity was evaluated separately for inclusions of quartz and calcite in other minerals (garnet or forsterite) and for quartz and calcite grains in the matrix of the same sample. The 95% confidence level used in the criterion for homogeneity allows for one outlier in samples in which 20-39 analyses were made of the same mineral (the maximum number of analyses of the same mineral in a sample was 34, Table 2). Results for samples in which 20 or more analyses were made of the same mineral that were judged not homogeneous, however, all involve two or more outliers (Table 2).

Calculation of the MSWD of a group of analyses of the same mineral requires careful choice of the SD of each measurement. Following recent developments in reporting data in radiogenic isotope geochemistry, we define two different SDs. Type 1 SD, SD(1), only considers uncertainty in the raw $\delta^{18}O$ of an unknown mineral. Following Kita et al. (2009), SD(1) was based on the standard deviation of eight measurements of the working standard that bracket a group of typically ten measurements of unknowns (four measurements before, four after). Type 2 SD, SD(2), addi-

Table 2
Summary of oxygen isotope compositions measured by ion microprobe analysis.

A. Contact metamorphic rocks

Sample	B1W	B1W	B1W	B43A	B43A	B43A	CL30O	CL30O
Mineral[a]	Fo	Cal	Dol	Fo	Cal	Dol	Wo	Di
Number analyses	22	10	10	32	11	15	15	10
Range $\delta^{18}O$ (‰)	9.8–17.2	17.5–20.2	18.4–19.2	11.4–14.8	15.8–17.9	17.0–18.2	8.1–9.3	10.1–11.7
Type 1 2SD (‰)[b]	0.26–0.33	0.33	0.32	0.21–0.23	0.31	0.52–0.72	0.12–0.22	0.24
Type 2 2SD (‰)[b]	0.31–0.39	0.43	0.43	0.26 to 0.28	0.39	0.61–0.79	0.26–0.32	0.28
Homogeneity[c]	NH	NH	H	NH	NH	H	NH	NH
Largest homo grp[d]	14	8	10	11	7	15	10	8
Wt. mean (±2SE)[e]	10.79 ± 0.09	19.72 ± 0.16	18.76 ± 0.14	12.21 ± 0.07	16.30 ± 0.15	17.44 ± 0.17	8.64 ± 0.09	10.23 ± 0.10
Area (mm^2)[f]	8	3	12	26	4	80	24	41

Sample	CL30O	CL30O	G1A	G1A	G1A	KP1B	KP1B	KP1B
Mineral[a]	Kfs	Qtz	Fo	Cal (Mtx)	Cal (Inc)	Fo	Di	Cal (Mtx)
Number analyses	13	27	10	10	5	19	20	27
Range $\delta^{18}O$ (‰)	12.5–13.5	14.2–15.4	14.8–15.8	17.6–18.4	17.4–18.4	18.2–19.4	18.0–19.0	21.3–22.1
Type 1 2SD (‰)[b]	0.22	0.12–0.25	0.26–0.32	0.25	0.25	0.13–0.30	0.13–0.30	0.17–0.27
Type 2 2SD (‰)[b]	0.27	0.17–0.29	0.30–0.36	0.34	0.34	0.20–0.34	0.23–0.35	0.32–0.39
Homogeneity[c]	NH	NH	NH	NH	NH	NH	NH	H
Largest homo grp[d]	11	14	18	9	3	11	17	27
Wt. mean (±2SE)[e]	13.17 ± 0.08	14.81 ± 0.06	15.52 ± 0.08	17.92 ± 0.11	18.13 ± 0.20	19.05 ± 0.09	18.71 ± 0.07	21.68 ± 0.07
Area (mm^2)[f]	43	90	80	79	–	78	52	141

Sample	KP1B	KP1B	KP1K	KP1L	KP1L	KP1L	KP3E	KP3E
Mineral[a]	Cal (Inc)	Dol	Dol	Fo	Cal	Dol	Wo	Di
Number analyses	3	10	20	20	15	20	10	10
Range $\delta^{18}O$ (‰)	21.4–21.6	20.9–21.4	4.7–5.4	5.8–6.8	10.9–11.6	9.0–19.6	15.4–16.3	15.8–16.3
Type 1 2SD (‰)[b]	0.27	0.17–0.27	0.33–0.50	0.17–0.26	0.47–0.53	0.27–0.39	0.16	0.32
Type 2 2SD (‰)[b]	0.37–0.38	0.31–0.38	0.43–0.57	0.23–0.30	0.54–0.60	0.38–0.47	0.28	0.36
Homogeneity[c]	H	H	H	NH	H	NH	NH	H
Largest homo grp[d]	3	10	20	13	15	15	6	10
Wt. mean (±2SE)[e]	21.50 ± 0.22	21.17 ± 0.11	5.10 ± 0.11	6.51 ± 0.07	11.26 ± 0.15	19.09 ± 0.11	15.69 ± 0.10	16.04 ± 0.11
Area (mm^2)[f]	–	10	26	47	43	53	46	2

Sample	KP3E	KP3E	KP3E	KP3E	KP3E
Mineral[a]	Grs	Kfs	Pl	Qtz	Cal
Number analyses	10	10	10	10	10
Range $\delta^{18}O$ (‰)	14.8–15.6	19.3–19.6	17.1–17.6	20.4–21.5	19.6–20.1
Type 1 2SD (‰)[b]	0.23	0.27	0.18	0.20	0.29
Type 2 2SD (‰)[b]	0.31	0.32	0.24	0.25	0.37
Homogeneity[c]	NH	H	H	NH	H
Largest homo grp[d]	9	10	10	6	10
Wt. mean (±2SE)[e]	15.39 ± 0.10	19.45 ± 0.10	17.38 ± 0.08	20.60 ± 0.09	19.92 ± 0.12
Area (mm^2)[f]	7	1	1	3	56

B. Regional metamorphic rocks

Sample	E6	E6	E6	E6	Gass	Gass	Gass	Q1d
Mineral[a]	Grt	Pl	Qtz	Ky	Grt	Qtz	Ky	Pl
Number analyses	20	10	18	12	20	19	10	10
Range $\delta^{18}O$ (‰)	5.2–6.4	8.3–8.8	10.1–10.9	7.2–7.7	10.7–11.5	15.4–16.2	12.6–12.8	12.8–13.3
Type 1 2SD (‰)[b]	0.29–0.31	0.14	0.30–0.32	0.30–0.31	0.28–0.32	0.21–0.26	0.29	0.19
Type 2 2SD (‰)[b]	0.61–0.63	0.23	0.35–0.36	0.35–0.36	0.60–0.63	0.28–0.31	0.36	0.27
Homogeneity[c]	H	NH	NH	H	H	NH	H	H
Largest homo grp[d]	20	9	17	12	20	17	10	10
Wt. mean (±2SE)[e]	5.79 ± 0.14	8.58 ± 0.08	10.55 ± 0.08	7.50 ± 0.10	11.16 ± 0.14	15.62 ± 0.07	12.65 ± 0.11	13.06 ± 0.08
Area (mm^2)[f]	44	6	78	88	18	88	1	3

Sample	Q1d	Q1d	Q1J	Q1J	Q2A	Q2A	Q2A	Q2A
Mineral[a]	Qtz	Cal	Qtz	Cal	Grt	Pl	Qtz (Mtx)	Qtz (Inc)
Number analyses	10	10	10	10	20	6	18	15
Range $\delta^{18}O$ (‰)	15.7–16.1	15.4–16.1	16.0–16.6	15.5–16.1	10.0–10.5	12.3–13.0	14.5–14.9	14.1–14.8
Type 1 2SD (‰)[b]	0.19	0.31	0.27	0.24	0.38–0.47	0.11–0.23	0.11–0.32	0.23–0.32
Type 2 2SD (‰)[b]	0.24	0.40	0.34	0.34	0.65–0.71	0.21–0.29	0.17–0.35	0.27–0.35
Homogeneity[c]	H	H	H	H	H	NH	NH	NH
Largest homo grp[d]	10	10	10	10	20	5	16	14
Wt. mean (±2SE)[e]	15.90 ± 0.08	15.77 ± 0.13	16.34 ± 0.11	15.84 ± 0.11	10.28 ± 0.15	12.60 ± 0.11	14.63 ± 0.05	14.43 ± 0.08
Area (mm^2)[f]	10	10	22	19	45	12	77	–

Table 2 (continued)

Sample	3-4F	3-4G	3-4G	3-4G	3-4G	3-4G	21-24C	21-24C
Mineral[a]	Di	Di	Kfs	Pl	Qtz	Cal	Grt	Pl
Number analyses	12	20	10	10	20	20	13	11
Range $\delta^{18}O$ (‰)	7.3–8.7	7.8–8.7	9.6–10.2	8.9–9.8	11.9–12.6	9.8–10.5	8.5–9.2	10.5–11.2
Type 1 2SD (‰)[b]	0.18	0.29–0.39	0.20	0.18	0.25–0.33	0.20–0.28	0.14–0.24	0.17
Type 2 2SD (‰)[b]	0.22	0.32–0.41	0.26	0.25	0.28–0.36	0.30–0.36	0.54–0.58	0.25
Homogeneity[c]	NH	NH	NH	NH	H	H	H	NH
Largest homo grp[d]	7	18	9	9	20	20	13	10
Wt. mean (±2SE)[e]	7.83 ± 0.08	8.11 ± 0.08	9.81 ± 0.09	9.18 ± 0.08	12.22 ± 0.07	10.14 ± 0.07	8.83 ± 0.16	10.63 ± 0.08
Area (mm²)[f]	2	99	108	1	77	118	11	13

Sample	21-24C	21-24C	21-24C	21-24C	21-25C	21-25C	21-25C	21-25C
Mineral[a]	Qtz (Mtx)	Qtz (Inc)	Cal (Mtx)	Cal (Inc)	Grt	Pl	Qtz (Mtx)	Qtz (Inc)
Number analyses	10	17	10	10	20	10	10	20
Range $\delta^{18}O$ (‰)	13.7–14.3	13.5–14.0	13.4–13.9	13.2–13.9	9.8–10.3	11.7–12.8	14.6–15.1	14.4–14.7
Type 1 2SD (‰)[b]	0.14–0.29	0.14–0.29	0.24–0.30	0.24–0.30	0.25–0.40	0.20	0.25–0.40	0.30–0.40
Type 2 2SD (‰)[b]	0.23–0.34	0.23–0.34	0.33–0.38	0.33–0.38	0.58–0.66	0.27–0.28	0.31–0.44	0.35–0.44
Homogeneity[c]	NH	H	H	H	H	NH	H	H
Largest homo grp[d]	8	17	10	10	20	5	10	20
Wt. mean (±2SE)[e]	13.92 ± 0.09	13.71 ± 0.07	13.65 ± 0.11	13.53 ± 0.11	10.10 ± 0.14	12.47 ± 0.12	14.84 ± 0.11	14.52 ± 0.09
Area (mm²)[f]	12	–	10	–	75	12	64	–

Sample	21-25C	21-25C	21-25J	21-25J	21-25J	21-26E	21-26E	21-26E
Mineral[a]	Cal (Mtx)	Cal (Inc)	Pl	Qtz	Cal	Grt	Pl	Qtz
Number analyses	15	5	11	17	15	10	10	10
Range $\delta^{18}O$ (‰)	14.4–15.0	13.9–14.2	11.6–12.5	14.4–15.2	14.0–14.7	12.0–12.4	14.9–15.5	17.2–17.7
Type 1 2SD (‰)[b]	0.25	0.24	0.17	0.12–0.14	0.41	0.16–0.24	0.19	0.16–0.24
Type 2 2SD (‰)[b]	0.33	0.34	0.24	0.17–0.19	0.49	0.55–0.58	0.27	0.24–0.30
Homogeneity[c]	H	H	NH	NH	H	H	NH	NH
Largest homo grp[d]	15	5	9	13	15	10	9	9
Wt. mean (±2SE)[e]	14.66 ± 0.09	14.05 ± 0.15	12.38 ± 0.08	14.60 ± 0.05	14.37 ± 0.13	12.08 ± 0.18	15.13 ± 0.09	17.50 ± 0.08
Area (mm²)[f]	53	–	25	41	11	54	68	36

Sample	21-26E	21-28A	21-28A	21-28A	21-28A	21-29C	21-29C	21-29G
Mineral[a]	Cal	Grt	Pl	Qtz (Mtx)	Qtz (Inc)	Qtz (Mtx)	Qtz (Inc)	Qtz (Mtx)
Number analyses	10	20	10	20	21	4	8	14
Range $\delta^{18}O$ (‰)	16.9–17.8	11.1–11.7	14.4–15.0	16.2–17.0	15.5–16.6	13.1–13.3	13.0–13.2	13.4–14.3
Type 1 2SD (‰)[b]	0.19	0.24–0.30	0.18–0.21	0.18–0.21	0.19–0.22	0.21	0.21	0.22–0.27
Type 2 2SD (‰)[b]	0.30	0.58–0.61	0.25–0.27	0.22–0.25	0.23–0.26	0.24	0.24	0.24–0.29
Homogeneity[c]	NH	H	NH	NH	NH	H	H	NH
Largest homo grp[d]	9	20	9	17	17	4	8	12
Wt. mean (±2SE)[e]	17.28 ± 0.10	11.45 ± 0.13	14.64 ± 0.09	16.55 ± 0.06	16.13 ± 0.06	13.20 ± 0.12	13.11 ± 0.08	13.62 ± 0.07
Area (mm²)[f]	58	18	3	29	–	<1	–	21

Sample	21-29G	34-1A	34-1A	34-1A	34-1A	34-1A
Mineral[a]	Qtz (Inc)	Di	Kfs	Pl	Qtz	Cal
Number analyses	34	19	10	10	20	20
Range $\delta^{18}O$ (‰)	12.9–13.7	16.2–16.8	18.3–18.7	17.2–17.6	20.5–21.0	18.2–19.0
Type 1 2SD (‰)[b]	0.22–0.27	0.23–0.32	0.23	0.27	0.23–0.32	0.26–0.31
Type 2 2SD (‰)[b]	0.24–0.29	0.26–0.34	0.27	0.33–0.34	0.26–0.35	0.34–0.38
Homogeneity[c]	NH	NH	H	H	H	H
Largest homo grp[d]	29	19	10	10	20	20
Wt. mean (±2SE)[e]	13.16 ± 0.05	16.46 ± 0.07	18.44 ± 0.09	17.37 ± 0.11	20.70 ± 0.07	18.50 ± 0.08
Area (mm²)[f]	–	106	58	118	102	106

[a] See footnotes to Table 1 for definition of mineral abbreviations. Mtx refers to grains in the matrix. Inc refers to inclusions in forsterite or garnet.

[b] Type 1 SD (standard deviation) is solely based on the standard deviation of 8 analyses of the working standard that bracket a group of unknowns. Type 2 SD considers the uncertainty in *bias**(*unknown*) as well (see Appendix A for details).

[c] Homogeneity of a given mineral in a sample was judged by the mean square weighted deviate (MSWD), calculated following Mahon (1996) and using Type 1 SD for Di, Fo, Kfs, Ky, Qtz, and Wo and Type 2 SD for Cal, Dol, Grt, and Pl. H = homogeneous at a 95% confidence level; otherwise, NH = not homogeneous.

[d] Number in largest homogenous group of analyses of the mineral in the sample, using the Type 2 SD.

[e] Weighted mean $\delta^{18}O$ of the largest homogenous group of analyses of the mineral in the sample, calculated following Mahon (1996) and using Type 2 SD. SE = standard error.

[f] Area of smallest circle that circumscribes all analyses of a given mineral in a given sample.

tionally considers the uncertainties in the non-canceling terms in $bias$(WS) and $bias$*($unknown$); uncertainty in the latter includes (in the case of calcite, dolomite, garnet, and plagioclase) the uncertainty in the chemical composition of the mineral at the site of ion probe analysis (determined by electron microprobe). Further details are provided in Appendix A.

The ranges in values of SD(1) and SD(2) for each analyzed mineral in each sample are listed in Table 2. The type 2 SD provides the best estimate of the uncertainty of the
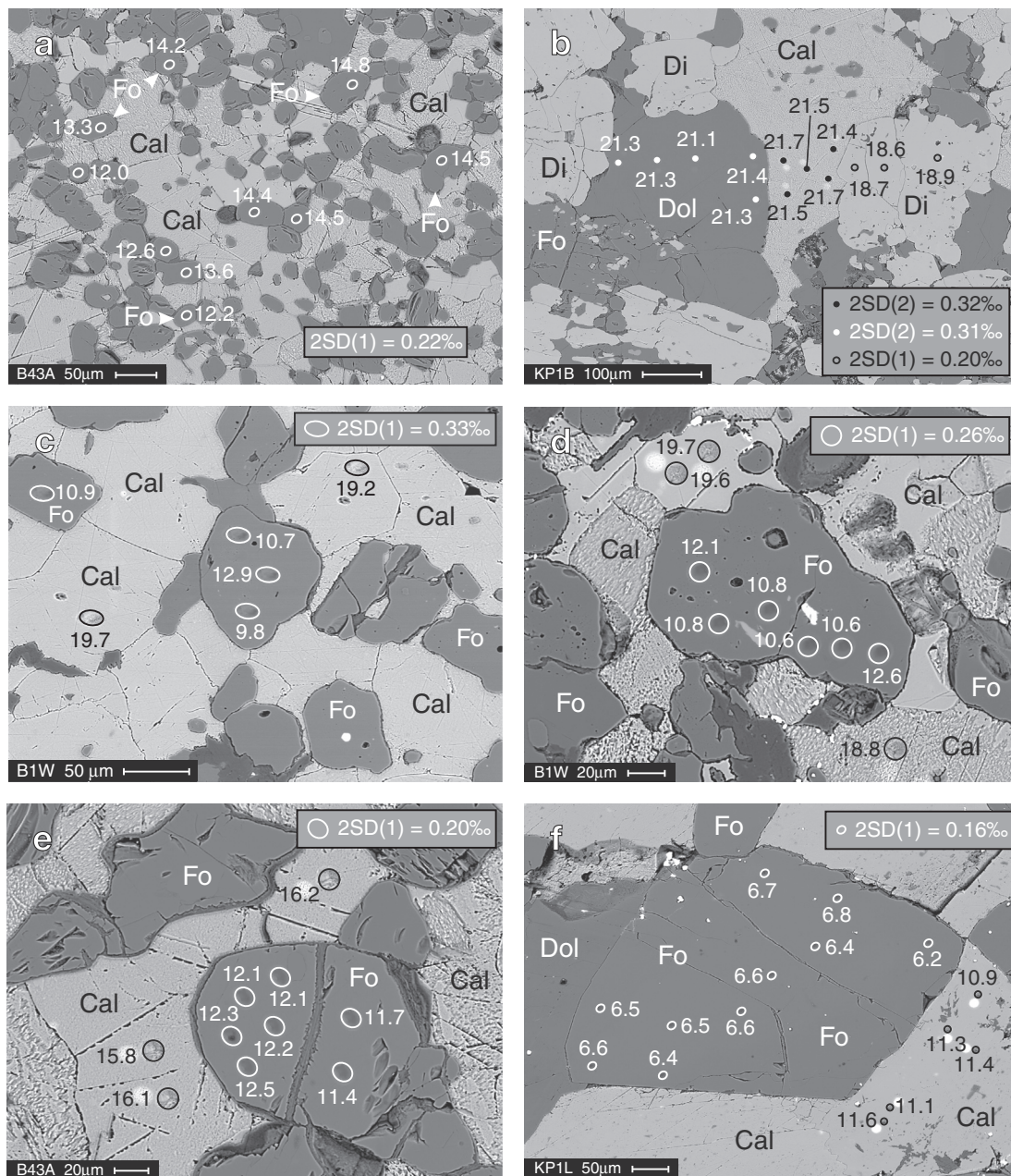
Fig. 2. BSE images of siliceous dolomite marble illustrating different examples of grain-to-grain and intracrystalline variation in $\delta^{18}O$ (‰, VSMOW) in fosterite (Fo), calcite (Cal), dolomite (Dol), and diopside (Di). Locations and sizes of ion microprobe analysis pits are shown as white and black ovals and circles. Bright spots next to calcite analysis pits are places where the C coat was destroyed during electron microprobe analysis. All forsterite grains have X_{Mg} = Mg/(Mg + Fe) > 0.99. (a) Sample B43A. The area shows the petrographic context of a grain-to-grain variability in $\delta^{18}O$ of 2.8‰ in forsterite over a distance of ~400 μm. (b) Sample KP1B. The area illustrates the strategy for evaluating intracrystalline variability in $\delta^{18}O$ in coexisting minerals. (c) Sample B1 W. The forsterite grain that exhibits the greatest variability in $\delta^{18}O$ of any silicate grain in the entire study has $\delta^{18}O$ higher in the interior than at the edge. (d) Sample B1W. A second forsterite grain has $\delta^{18}O$ higher at the grain ends than in the interior. (e) Sample B43A. A forsterite grain has $\delta^{18}O$ significantly different in two parts separated by a serpentine-filled fracture. (f) Sample KP1L. The larger forsterite grain is homogeneous in $\delta^{18}O$ except along one edge where maximum and minimum values are separated by ~100 μm.

$\delta^{18}O$ of analyzed minerals on the VSMOW scale. For minerals that are pure substances and for mineral solid solutions whose *bias**(*unknown*) corrections are independent of composition, however, the *bias*(WS) and *bias**(*unknown*) terms cancel in evaluations of measured differences in $\delta^{18}O$ among analyses of the same mineral in the same sample. In the evaluation of differences among values of $\delta^{18}O$ of the same mineral in the same sample, therefore, the more stringent type 1 SD was used to compute MSWD for kyanite, quartz, and wollastonite (pure substances) and for diopside, forsterite, and K-feldspar [*bias**(*unknown*) corrections independent of composition over the range of compositions of the unknowns]. Because *bias**(*unknown*) corrections for calcite, dolomite, garnet, and plagioclase depend on composition and because the chemical composition of these minerals can vary from grain to grain, differences in measured values of $\delta^{18}O$ between analysis spots of these minerals in the same sample depend on composition. Uncertainty in the dependence of *bias**(*unknown*) on mineral composition thus influences the status of the grain-scale homogeneity of calcite, dolomite, garnet, and plagioclase, and this uncertainty has been quantitatively accounted for. Specifi-

cally, in the evaluation of differences among values of $\delta^{18}O$ of calcite, dolomite, plagioclase, or garnet in the same sample, type 2 SD was used to compute MWSD.

4.1.2. Contact metamorphic rocks

Fig. 2a illustrates the strategy behind the evaluation of grain-to-grain variability in $\delta^{18}O$ of minerals. Analyses of $\delta^{18}O$ of multiple grains of the same mineral were made in small regions of interest, typically several hundred μm in diameter. Several different regions of interest were analyzed in most samples, but they occurred within the same 1.86 cm^2 or smaller area. The regions of interest were much larger than grain size in all samples. Grain-to-grain variability in $\delta^{18}O$ of analyzed minerals in contact metamorphic rocks is summarized in Table 3A and (with a single exception) on δ–δ diagrams in Fig. 3. The exception is dolomite in sample KP1K that is the only mineral analyzed in the sample. Data for mineral inclusions are omitted from Fig. 3. The edges of the boxes represent the measured range in $\delta^{18}O$ of analyzed minerals. The same range in measured $\delta^{18}O$ for the same mineral in different samples or for differ-

Table 3
Summary of degree of grain-to-grain homogeneity of analyzed minerals in $\delta^{18}O$.

Mineral[a]	No. samples	No. Homogeneous, all analyses[b]	No. Homogeneous, 1 outlier excluded[c]	Max diff $\delta \pm 2SD$[d]	Sample[e]
A. Contact metamorphic rocks					
Dol	5	4 (80%)	4 (80%)	10.61 ± 0.60	KP1L
Cal[f]	6	3 (50%)	4 (67%)	2.74 ± 0.45	B1W
Kfs	2	1 (50%)	1 (50%)	0.99 ± 0.31	CL30O
Di	3	1 (33%)	1 (33%)	1.57 ± 0.34	CL30O
Fo	5	0	0	7.40 ± 0.59	B1W
Grt	1	0	1 (100%)	0.81 ± 0.40	KP3E
Pl	1	0	1 (100%)	0.50 ± 0.34	KP3E
Qtz	2	0	0	1.21 ± 0.27	CL30O
Wo	2	0	0	1.23 ± 0.24	CL30O
Silicates	16	2 (13%)	4 (25%)		
Carbonates	11	7 (64%)	8 (73%)		
All minerals	27	8 (30%)	11 (41%)		
B. Regional metamorphic rocks					
Ky	2	2 (100%)	2 (100%)	–	
Grt	7	7 (100%)	7 (100%)	–	
Cal[f]	8	7 (88%)	8 (100%)	0.94 ± 0.42	21-26E
Kfs	2	1 (50%)	2 (100%)	0.60 ± 0.29	3-4G
Qtz[f]	14	6 (43%)	8 (57%)	0.83 ± 0.27	21-28A
Pl	10	2 (20%)	8 (80%)	1.08 ± 0.39	21-25C
Di	2	0	0	0.95 ± 0.46	3-4G
Silicates	37	18 (49%)	27 (73%)		
Carbonates	8	7 (88%)	8 (100%)		
All minerals	45	25 (56%)	35 (78%)		

[a] See footnotes to Table 1 for definition of mineral abbreviations.
[b] Number of samples in which all analyses of the mineral are statistically indistinguishable as judged by the criterion in the text and in the footnotes to Table 2. Percent of samples in which the mineral is homogeneous in parentheses.
[c] Number of samples in which all analyses of the mineral, or all analyses excluding one outlier, are statistically homogeneous as judged by the criterion in the text and in the footnotes to Table 2. Percent of samples is in parentheses.
[d] Maximum difference in $\delta^{18}O$ measured between two different grains of the same mineral in the same sample. SD(2) for Cal, Dol, Grt, and Pl; SD(1) for all other minerals.
[e] Sample that contains the mineral exhibiting the maximum range in $\delta^{18}O$.
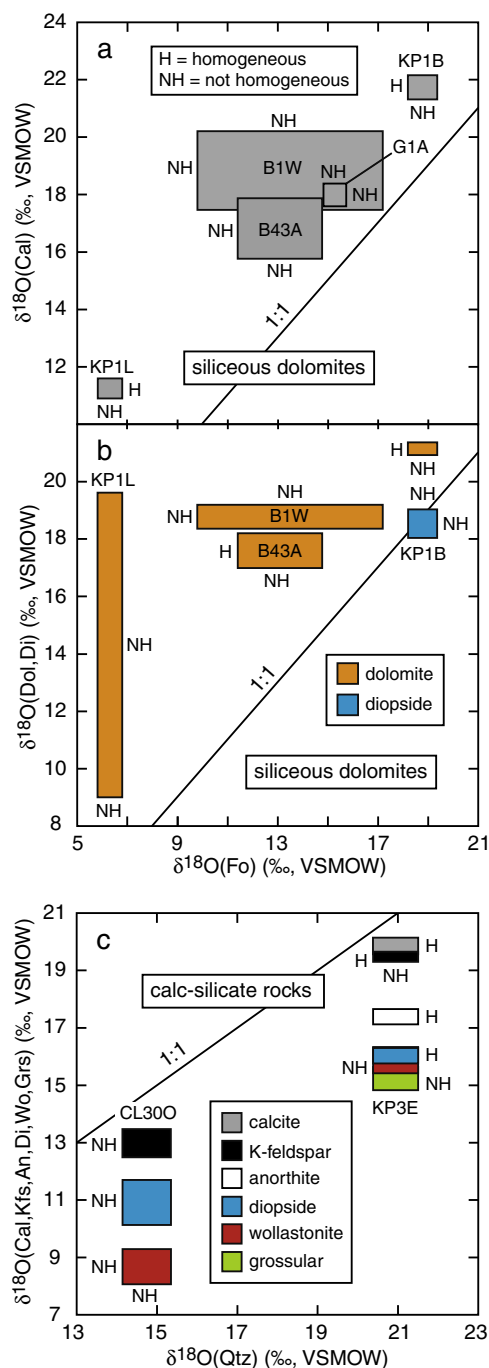[f] Matrix grains only.

Fig. 3. Summary of measured $\delta^{18}O$ of all analyzed minerals in contact metamorphosed rocks (except dolomite in sample KP1K). Data for mineral inclusions are omitted. Edges of boxes represent the measured range in $\delta^{18}O$ of each mineral. The "H" label next to the side of a box indicates that all analyzed grains of that mineral in a sample are homogeneous according to the criterion defined in the text. The "NH" label indicates that the mineral grains are not homogeneous. (a) and (b) Metamorphosed siliceous dolomites. (c) Calc-silicate rocks. Boxes for diopside, wollastonite, and grossular in sample KP3E overlap significantly.

ent minerals in the same sample may be judged as either homogeneous or inhomogeneous depending on the number of analyses of the mineral, the standard deviation of the

working standard during analysis, and the uncertainty in the bias*(unknown) correction.

Of all rock types analyzed, $\delta^{18}O$ is most variable in minerals from contact metamorphosed siliceous dolomite marbles (Fig. 3a and b). Of fifteen analyzed minerals in five samples of siliceous dolomite, only five are homogeneous, calcite in samples KP1B and KP1L and dolomite in samples B1W, B43A and KP1B. Neither forsterite nor diopside is homogeneous in any sample. As an example, Fig. 2a illustrates the petrographic setting of isotopically variable forsterite grains in sample B43A, all with $X_{Mg} = Mg/(Mg + Fe) > 0.99$. Ten different grains were analyzed; a maximum difference in $\delta^{18}O$ of $2.8 \pm 0.31\permil$ occurs between grains ~400 μm apart. (Reported uncertainties in differences are 2SD(1) or 2SD(2), as appropriate, added in quadrature.) The largest grain-to-grain variation in $\delta^{18}O$ observed in a silicate mineral, $7.4 \pm 0.47\permil$, is exhibited by forsterite grains in sample B1 W, all with $X_{Mg} > 0.99$ (Fig. 3a). The largest variation in $\delta^{18}O$ observed in a carbonate mineral, $10.6 \pm 0.45\permil$, is exhibited by dolomite grains in sample KP1L, all with $X^*_{Mg} = Mg/(Mg + Ca + Fe + Mn) = 0.48–0.49$ (Fig. 3b). In general, carbonate minerals are less variable than coexisting silicates. The obvious exception is dolomite in sample KP1L that has a range in $\delta^{18}O$ greater than any other mineral analyzed in the entire study.

The $\delta^{18}O$ of minerals in contact metamorphosed calc-silicate rocks is summarized in Fig. 3c. To facilitate comparison, all panels in Fig. 3 span $14\permil$ along the vertical axis. Of eleven analyzed minerals in two samples of contact metamorphosed calc-silicate rocks, only four are homogeneous: calcite, K-feldspar, anorthite, and diopside in sample KP3E. Grossular and wollastonite are not homogeneous. Nevertheless, as illustrated by the relative sizes of the boxes in Fig. 3, minerals in the calc-silicate rocks are generally less variable in $\delta^{18}O$ than minerals in the forsterite marbles. The largest grain-to-grain range in $\delta^{18}O$ exhibited by a mineral in calc-silicates rocks ($1.6 \pm 0.34\permil$ in diopside grains, sample CL30O) is considerably smaller than the largest range in $\delta^{18}O$ exhibited by calcite, forsterite, and dolomite grains in siliceous dolomite marbles.

Considering all analyzed grains in contact metamorphic rocks together, only 13% of analyzed silicate minerals and 64% of analyzed carbonate minerals are homogeneous over an area in each sample $\leqslant 1.41$ cm^2 (Table 3A). Grouping all carbonate and silicate minerals together, 30% are homogeneous. Results in Table 3A further evaluate the degree to which conclusions about mineral homogeneity are controlled by a single outlying analysis in a sample. The fourth column in Table 3A shows how conclusions would change if homogeneity were judged omitting the one analysis that deviates the most from the other analyses of a given mineral from a given sample. Omitting one outlying analysis changes the inferred degree of homogeneity of $\delta^{18}O$ in the samples only modestly.

4.1.3. Regional metamorphic rocks

Grain-to-grain variability in $\delta^{18}O$ of analyzed minerals in regional metamorphic rocks is summarized in Table 3B and (with three exceptions) on δ–δ diagrams in Fig. 4.

The exceptions are three samples for which data are reported for a single mineral (diopside in sample 3-4F and quartz in samples 21-29C and 21-29G). Data for min-
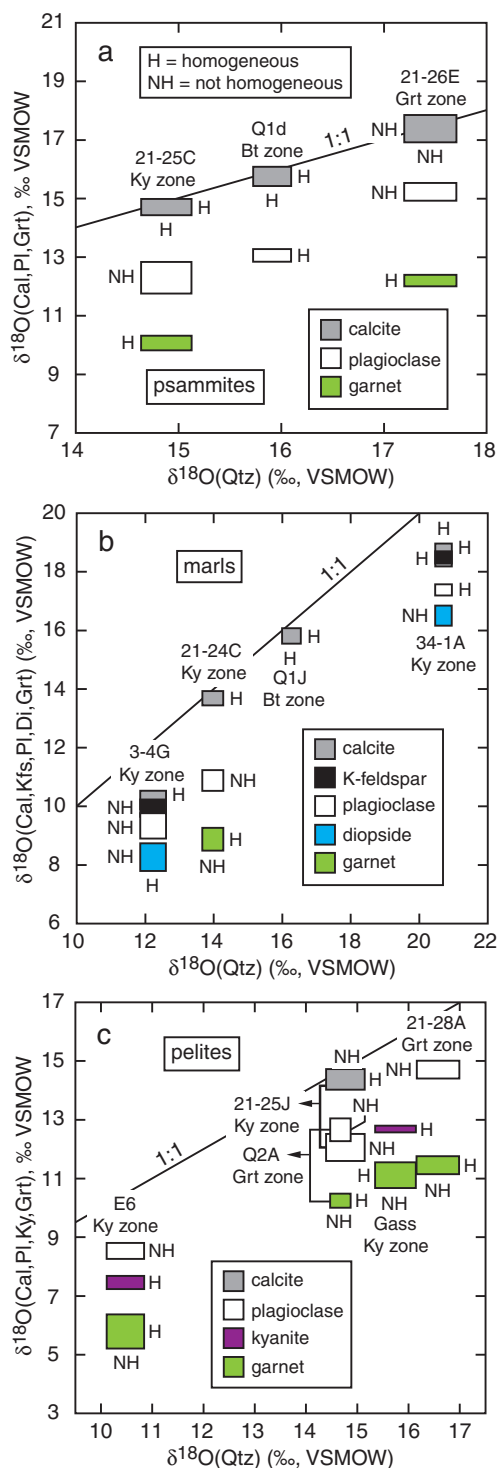

Fig. 4. Summary of measured $\delta^{18}O$ of all analyzed minerals in regional metamorphosed rocks (except diopside in sample 3-4F and quartz in samples 21-29C and 21-29G). The format is the same as in Fig. 3. Data for mineral inclusions are omitted. (a) Psammites. (b) Marls. Boxes for calcite and K-feldspar in samples 34-1A and 3-4G overlap significantly. (c) Pelites.

eral inclusions are omitted from Fig. 4. The edges of the boxes represent the measured range in $\delta^{18}O$ of analyzed minerals. To facilitate comparisons between Figs. 3 and 4, the vertical axis of all panels in both figures spans 14‰. Although minerals in regional metamorphic rocks are more homogeneous in $\delta^{18}O$ than minerals in contact metamorphic rocks, significant grain-to-grain variability does exist. Among eleven analyzed minerals in metamorphosed psammites from the biotite, garnet, and kyanite zones, four are not homogeneous: quartz, calcite, and plagioclase in garnet-zone sample 21-26E and plagioclase in kyanite-zone sample 21-25C (Fig. 4a). Among sixteen analyzed minerals in metamorphosed marls from the biotite and kyanite zones, six are not homogeneous: diopside in samples 3-4G and 34-1A, K-feldspar in sample 3-4G, plagioclase in samples 3-4G and 21-24C, and quartz in sample 21-24C (Fig. 4b). Among sixteen analyzed minerals in pelites from the garnet and kyanite zones, only seven are homogeneous: kyanite in samples E6 and Gass; garnet in samples 21-28A, Q2A, E6, and Gass; and calcite in sample 21-25J (Fig. 4c). The largest grain-to-grain variability in $\delta^{18}O$ measured of a mineral from a regional metamorphic rock (1.1 ± 0.39‰ in plagioclase from sample 21-25C) is much less than the variability in $\delta^{18}O$ observed in many minerals from contact metamorphic rocks. All of the other 44 analyzed minerals from regional metamorphic rocks exhibit grain-to-grain variability of <1‰. There is no systematic correlation between the degree of grain-to-grain homogeneity and either rock type or grade of metamorphism.

The greater degree of grain-to-grain homogeneity in $\delta^{18}O$ of minerals in regional metamorphic rocks, compared to that in contact metamorphic rocks, is further documented by results in Table 3B. Considering all the analyzed regional metamorphic rocks, 49% of analyzed silicate minerals, 88% of analyzed carbonate minerals, and 56% of silicate and carbonate minerals together are homogeneous over an area in each sample $\leqslant 1.18$ cm^2. Results in Table 3B further demonstrate that much of the variability in $\delta^{18}O$ of minerals in regional metamorphic rocks can be attributed to a single outlying analysis, particularly in the case of feldspar. Once a single outlying analysis is excluded, the percentage of homogeneous minerals increases to 73% among silicates, 100% among carbonates, and 78% among silicate and carbonate minerals together. Results in Table 3B are similar to those of Gordon et al. (2012) who found (with the exception of one sample) that grain-to-grain variations in $\delta^{18}O$ of kyanite, garnet, and quartz, measured by ion microprobe in eight samples of granulite and eclogite, were <~1‰.

4.2. Intracrystalline variability in oxygen isotope composition

A total of 232 different mineral grains were analyzed in two or more places (maximum 16 analyses/grain). The question whether the 232 grains were homogeneous or not in $\delta^{18}O$ was addressed by applying the same criterion used to evaluate grain-to-grain variability by calculating a MSWD for all analyses from the same grain (Section 4.1.1). Fig. 2b illustrates the strategy behind the evaluation of intracrystalline variability in $\delta^{18}O$ of minerals. In small

regions of interest, typically several hundred μm in diameter, traverses were made across groups of 2–4 different, adjacent mineral grains. Fig. 2b specifically illustrates a traverse across adjacent grains of dolomite, calcite, and diopside in sample KP1B. The traverses not only assess whether variability in $\delta^{18}O$ exists within minerals but also whether there are systematic differences in $\delta^{18}O$ between the edge and interior of grains and between contacts with different minerals.

4.2.1. Contact metamorphic rocks

Intracrystalline variability in $\delta^{18}O$ of minerals from contact metamorphic rocks is summarized in Table 4A. As the representative data in Fig. 2b illustrate, statistically significant variability in $\delta^{18}O$ within individual grains is atypical. Of 88 minerals analyzed in two or more spots, only 28 are not homogeneous. Only a small fraction of analyzed carbonate grains are not homogenous (3 of 37) while just less than half the silicate grains are not homogeneous (25 of 51). The largest intracrystalline variation in $\delta^{18}O$ within a sili-

Table 4
Summary of degree of intracrystalline homogeneity of analyzed minerals in $\delta^{18}O$.

Mineral[a]	$n(T) \geqslant 2$[b]	$n(NH) \geqslant 2$[c]	% Homog[d]	Max diff $\delta \pm 2SD$[e]	Sample[f]
A. Contact metamorphic rocks					
Pl	3	0	100	–	
Dol	15	1	93	10.12 ± 0.54	KP1L
Cal	22	2	91	1.36 ± 0.64	B1W
Kfs	7	2	71	0.70 ± 0.31	CL30O
Fo	19	9	53	3.10 ± 0.47	B1W
Di	8	4	50	1.72 ± 0.34	CL30O
Wo	8	5	38	0.67 ± 0.16	CL30O
Qtz	6	5	17	1.21 ± 0.27	CL30O
Silicates	51	25	51		
Carbonates	37	3	92		
All minerals	88	28	68		
B. Regional metamorphic rocks					
Grt	14	0	100	–	
Kfs	5	0	100	–	
Ky	4	0	100	–	
Cal	29	1	97	0.74 ± 0.43	21-26E
Pl	26	2	92	0.87 ± 0.36	3-4G
Qtz	55	5	91	0.50 ± 0.19	21-25J
Diop	11	1	91	1.49 ± 0.25	3-4F
Silicates	115	8	93		
Carbonates	29	1	97		
All minerals	144	9	94		

Mineral[a]	Sample	Figure	Max diff $\delta \pm 2SD$[e]	No. analyses	Comments on zonation pattern
C. Zonation patterns in individual grains[g]					
Di	KP1B	–	0.66 ± 0.34	5	δ edge > δ interior
Di	3-4F	7c	1.49 ± 0.25	12	δ edge > δ interior
Di	3-4G	–	0.73 ± 0.39	5	Highest δ at edge
Dol	KP1L	7a	10.12 ± 0.54	9	No systematic pattern
Fo	B1W	6a	3.10 ± 0.47	3	δ edge < δ interior
Fo	B1W	6b	2.03 ± 0.36	6	δ at ends > δ in middle
Fo	B43A	6c	1.06 ± 0.28	7	δ one half > δ other half
Fo	KP1L	6d	0.63 ± 0.22	10	Highest and lowest δ at one edge
Qtz	21-28A	–	0.44 ± 0.28	5	δ edge > δ interior
Qtz	CL30O	7d	1.21 ± 0.27	16	δ edge > δ interior
Wo	KP3E	–	0.61 ± 0.22	5	δ edge > δ interior

[a] See footnotes to Table 1 for definition of mineral abbreviations.
[b] Number of individual grains of each mineral in all samples analyzed at two or more points.
[c] Number of individual grains of each mineral in all samples analyzed at two or more points that are not homogeneous as judged by the same criterion given in the text and in the footnotes to Table 2.
[d] Percent of grains analyzed at two or more points that are homogeneous as judged by the same criterion given in the text and in the footnotes to Table 2.
[e] Maximum difference in $\delta^{18}O$ measured within a single grain of each mineral. SD(2) for Cal, Dol, Grt, and Pl; SD(1) for all other minerals.
[f] Sample that contains the mineral grain exhibiting the maximum range in $\delta^{18}O$.
[g] All grains with $\geqslant 5$ analyses and exhibiting a discernable pattern plus the Fo grain from sample B1W and the Dol grain from sample KP1L with the largest measured range in $\delta^{18}O$ for a silicate and carbonate, respectively.
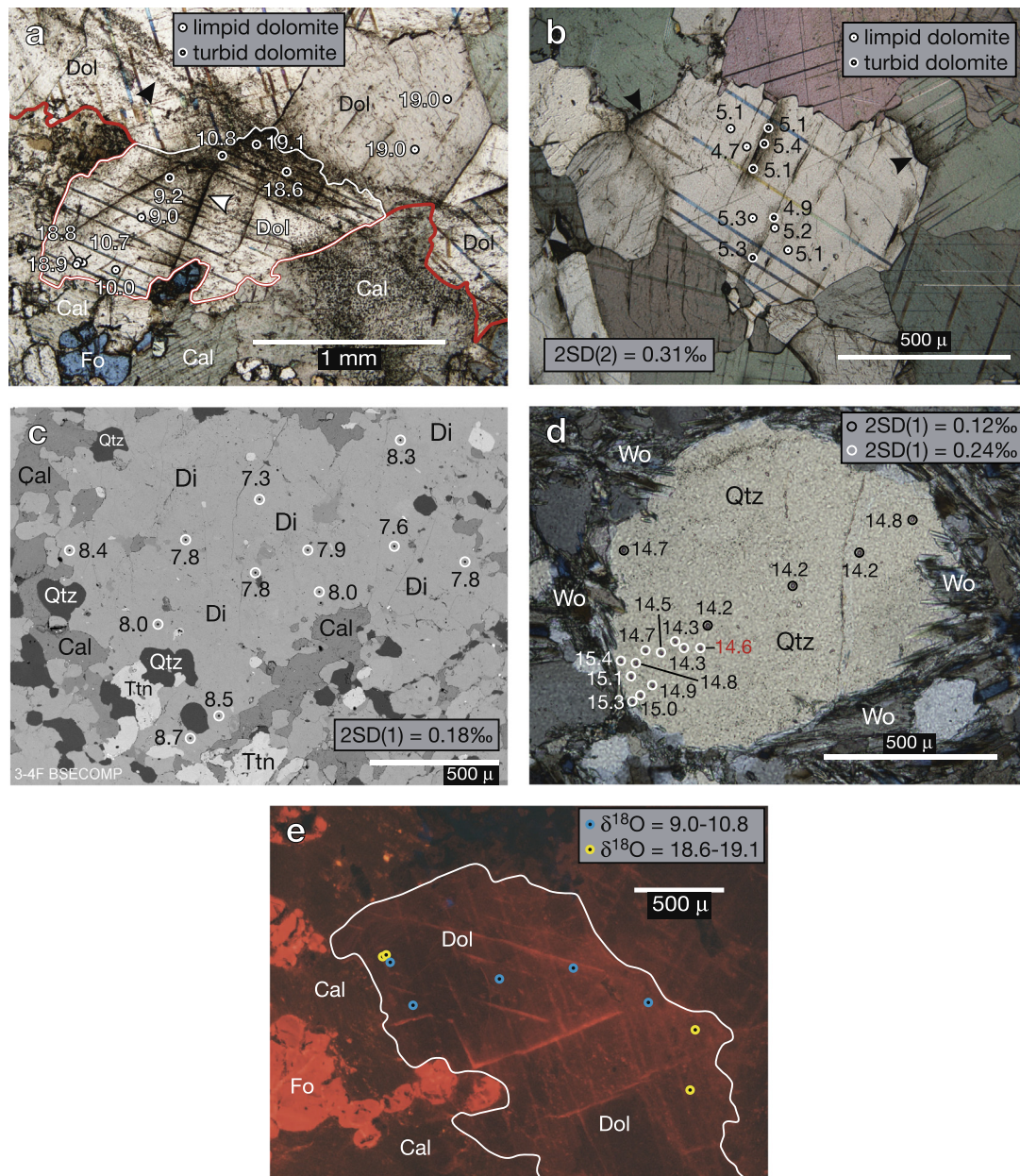
Fig. 5. Optical (crossed polarizers), BSE, and CL images of selected samples illustrating different examples of intracrystalline variation in $\delta^{18}O$ in dolomite (Dol), diopside (Di), and quartz (Qtz). Cal is calcite, Fo is forsterite, Ttn is titanite, and Wo is wollastonite. Analysis pits have location and size indicated by tiny white or black dots surrounded by a larger ring. Numbers are $\delta^{18}O$ (‰, VSMOW). (a) Optical image of sample KP1L. The dolomite grain (outlined in white) that exhibits the greatest variability in $\delta^{18}O$ of any mineral grain in the entire study has $\delta^{18}O$ differing by ~8‰ between spots 10–20 μm apart. Red curve is the contact between dolomite wall rock (above) and a cm-thick cross-cutting forsterite-calcite vein (below). Black arrow points to curved bands of turbidity that cut across cleavage and grain boundaries. White arrow points to a zone of turbidity along a cleavage plane. (b) Optical image of sample KP1K. Zones of turbidity are identified along some grain boundaries (by black arrows) and along cleavage planes (by analysis sites surrounded by a white ring). Measured values of $\delta^{18}O$ in turbid and limpid dolomite are statistically indistinguishable. (c) BSE image of sample 3-4F. The optically continuous diopside grain that exhibits the greatest variability in $\delta^{18}O$ of any mineral grain in all samples of regional metamorphic rock. Measured $\delta^{18}O$ at the edge of the grain is up to 1.4‰ greater than in the interior of the grain. (d) Optical image of sample CL30O. Quartz grain systematically zoned in $\delta^{18}O$ from a broad interior region with 14.2‰ to 15.4‰ at the edge. The value of $\delta^{18}O$ in red identifies the somewhat anomalous datum in Fig. 15 at $d/r = 0.46$. (e) CL image of sample KP1L. Same dolomite grain outlined in white as in panel (a) in different orientation. There is no systematic spatial pattern in CL brightness that correlates with differences in measured $\delta^{18}O$ values of dolomite. (For interpretation of the references to colour in this figure legend, the reader is referred to the web version of this article.)

cate mineral grain is $3.1 \pm 0.47‰$ in forsterite from sample B1W (Fig. 2c). Seven other silicate grains, including diopside and quartz as well as forsterite, exhibit variability in the range 1–2‰. Although the largest intracrystalline variation in $\delta^{18}O$ was measured in a dolomite grain from sample KP1L ($10.12 \pm 0.54‰$, Fig. 5a), only two out of the other 36 analyzed carbonate grains from contact metamorphic rocks are inhomogeneous. A surprising degree of intracrystalline $\delta^{18}O$ homogeneity of carbonate grains in contact metamorphosed dolomites from the periclase zone of the Alta aureole, Utah, was similarly observed by Bowman et al. (2009) who did not find a single inhomogeneous grain over a 10-cm traverse across calcite-dolomite marble along which $\delta^{18}O$ changed by 7‰.

4.2.2. Regional metamorphic rocks

Intracrystalline variability in $\delta^{18}O$ of minerals from regional metamorphic rocks is summarized in Table 4B. Mineral grains in regional metamorphic rocks are even more homogeneous in $\delta^{18}O$ than are grains in contact metamorphic rocks. Of 144 minerals analyzed in two or more spots, only nine are not homogeneous. Only a single carbonate grain out of 29 analyzed is not homogenous while only eight of 115 analyzed silicate grains are not homogeneous. More than 90% of the analyzed grains of diopside, the most variable mineral analyzed in regional metamorphic rocks, are homogeneous. The largest intracrystalline variation in $\delta^{18}O$ within a silicate mineral is $1.5 \pm 0.25‰$ in diopside from sample 3-4F (Table 4B, Fig. 5c). No other silicate grain exhibits variability in $\delta^{18}O > 1‰$. The range in $\delta^{18}O$ within the single inhomogeneous calcite grain (sample 21-26E) is $0.7 \pm 0.43‰$. Gordon et al. (2012) likewise found that intracrystalline variations in $\delta^{18}O$ of a given mineral in eight samples of granulite and eclogite were much smaller than grain-to-grain variations. All fourteen analyzed garnet grains from seven samples of regional metamorphic rock in this study are homogeneous in $\delta^{18}O$ within error of measurement (Table 4B). Raimondo et al. (2012) similarly reported ion microprobe analyses of garnets in amphibolite facies rocks that are either homogeneous in $\delta^{18}O$ within error of measurement or exhibit significant intracrystalline variations of no more than ~0.5‰. Larger intracrystalline variations in $\delta^{18}O$ of up to 9–10‰ in garnet from regional metamorphic rocks documented by other ion microprobe studies (Martin et al., 2011, 2014; Page et al., 2014) appear to be exceptional.

As a generalization, minerals exhibit much less intracrystalline variability in $\delta^{18}O$ in regional than in contact metamorphic rocks (Table 4). Because 94% of the 144 grains investigated in regional metamorphic rocks are unzoned in $\delta^{18}O$ within error of measurement (Table 4B), unfortunately, no meaningful general conclusions can be drawn about possible correlations between the occurrence of zoning and either rock type or grade of metamorphism.

4.2.3. Spatial patterns of oxygen isotope zonation within mineral grains

Consistent, systematic, spatial patterns of zonation of $\delta^{18}O$ in mineral grains from metamorphic rocks are surprisingly elusive. Representative examples are given in

Table 4C and Figs. 2 and 5. The forsterite grain from sample B1W that exhibits the largest intracrystalline range in $\delta^{18}O$ among silicates (Fig. 2c) appears to be zoned with $\delta^{18}O$ decreasing from the interior to the edge. Another forsterite grain in the same sample, however, is elongated with higher $\delta^{18}O$ at the ends of the grain than in the middle (Fig. 2d). Forsterite from a second sample (B43A) from the same contact aureole is split by a serpentine-filled fracture with homogeneous but significantly different values of $\delta^{18}O$ on either side (Fig. 2e). A forsterite grain from sample KP1L from another contact aureole is homogeneous except along one edge where maximum and minimum vales of $\delta^{18}O$ are separated by ~100 μm (Fig. 2f).

Another example of elusive zoning patterns is the dolomite grain from sample KP1L that exhibits the largest intracrystalline range in $\delta^{18}O$ among all analyzed minerals (Fig. 5a). The dolomite grain with variable $\delta^{18}O$ protrudes into a cross-cutting forsterite-calcite vein in which calcite and forsterite have much lower $\delta^{18}O$ (~11–12‰ and ~6–7‰, respectively, Table 2A) than dolomite wall rock away from the vein (~19–20‰, Fig. 5a; Table 2A). Low $\delta^{18}O$ regions in the inhomogeneous dolomite grain certainly are related to the formation of the forsterite-calcite vein. Values of $\delta^{18}O$ of dolomite in the grain, however, display no simple and consistent spatial relationship to the dolomite-vein contact. Measured $\delta^{18}O$ in the inhomogeneous dolomite grain can vary by up to ~8‰ between analysis spots separated by no more than ~10–20 μm (Fig. 5a).

Results in Figs. 2 and 5 indicate that definite intracrystalline zonation patterns in $\delta^{18}O$ normally emerge only when at least ten analyses are measured per grain. Two examples are illustrated in Fig. 5. Twelve analyses of the diopside grain from sample 3-4F, that exhibits the largest intracrystalline range in $\delta^{18}O$ among all analyzed minerals in regional metamorphic rocks, define a spatial pattern with higher values of $\delta^{18}O$ at the edge than in the grain interior (Fig. 5c). Five analyses of a large detrital quartz clast in sample CL30O made during one analytical session suggested that the grain was zoned with $\delta^{18}O$ increasing from core to rim (black rings, Fig. 5d). An additional eleven analyses of the same grain during a later session (white rings, Fig. 5d) confirm, albeit with poorer precision, a systematic outward increase in $\delta^{18}O$ by ~1.2‰ in a region near the rim that surrounds an interior with uniform $\delta^{18}O \approx 14.2‰$.

4.3. Matrix-inclusion relations

Calcite and quartz commonly occur both in the matrix of a rock and as inclusions in forsterite (calcite) and garnet (calcite and quartz). Inclusions of calcite and quartz in fifteen grains from eight samples were analyzed to determine if $\delta^{18}O$ systematically differed between the occurrence of calcite and quartz as inclusions and their occurrence in nearby matrix.

4.3.1. Calcite inclusions in forsterite and garnet

Calcite inclusions in forsterite from contact metamorphic rocks can have significantly higher X^*_{Mg} than calcite in the adjacent matrix (Ferry, 2001). Fig. 6a illustrates an
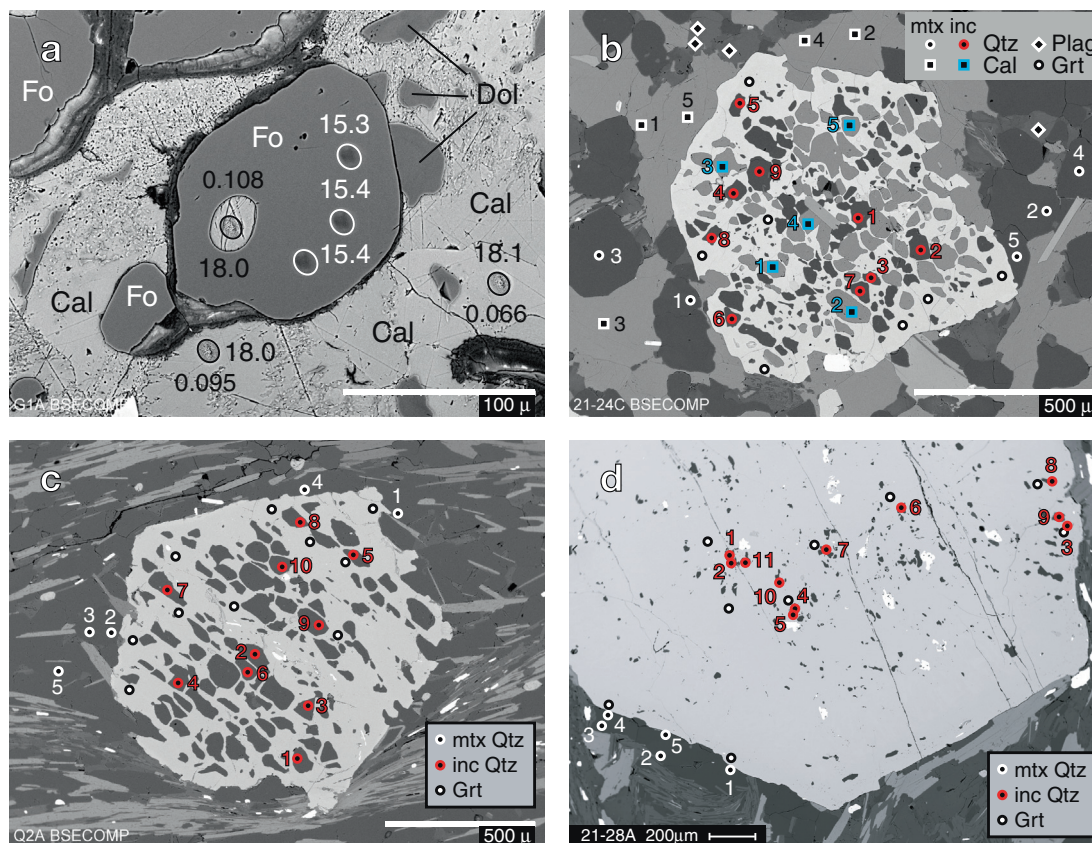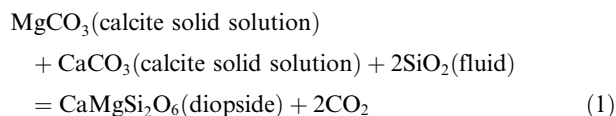
Fig. 6. BSE images showing locations of ion microprobe analyses of calcite (Cal) and quartz (Qtz) inclusions, of host forsterite (Fo) and garnet (Grt), and of nearby matrix calcite, quartz, and plagioclase (Pl). Dol is dolomite. Except in panel (a), analysis pits have location and size indicated by tiny white or black symbols surrounded by a larger circle, square, or diamond. (a) Sample G1A. Analysis pits have the same size and shape as the ovals. Numbers in the range 15–19 are measured values of $\delta^{18}O$ (‰, VSMOW). Numbers < 0.2 are X^*_{Mg} = Mg/(Ca + Mg + Fe + Mn) of calcite. Although X^*_{Mg} of matrix and inclusion calcite may differ, the $\delta^{18}O$ values of matrix and inclusion calcite are statistically indistinguishable. (b) Sample 21-24C, garnet A. Note difference in grain size between inclusion and matrix grains. Matrix calcite and quartz and inclusion calcite and quartz have $\delta^{18}O$ keyed by number to those in Figs. 8a and 10a. (c) Sample Q2A, garnet B. Note difference in orientation of foliation defined by quartz and ilmenite (white) inclusions in garnet and by matrix grains. Matrix and inclusion quartz have $\delta^{18}O$ keyed by number to those in Fig. 9a. (d) Sample 21-28A, garnet A. Matrix and inclusion quartz have $\delta^{18}O$ keyed by number to those in Fig. 10d.

example from sample G1A. Calcite inclusions in forsterite were analyzed in samples G1A and KP1B to determine if there are differences in $\delta^{18}O$ between inclusion and matrix that correlate with differences in X^*_{Mg}. One calcite inclusion in each of five grains of forsterite that have X^*_{Mg} in the range 0.106–0.117 and ten nearby matrix calcite grains that have lower X^*_{Mg} = 0.064–0.096 were analyzed for $\delta^{18}O$ in sample G1A. The lower X^*_{Mg} in matrix calcite in sample G1A resulted from exsolution of dolomite during cooling (Fig. 6a). One calcite inclusion in each of three grains of forsterite and seven adjacent matrix calcite grains were analyzed for $\delta^{18}O$ in sample KP1B. Two analyzed calcite inclusions in sample KP1B have X^*_{Mg} in the range 0.057–0.059 while the third inclusion and the seven matrix calcite grains adjacent to the forsterite grains have much lower X^*_{Mg} = 0.013–0.024. Matrix calcite in sample KP1B exhibits no textural evidence for exsolution of dolomite. The lower X^*_{Mg} of matrix calcite is likely the result of the reaction,

$$MgCO_3(\text{calcite solid solution})$$
$$+ CaCO_3(\text{calcite solid solution}) + 2SiO_2(\text{fluid})$$
$$= CaMgSi_2O_6(\text{diopside}) + 2CO_2 \qquad (1)$$

that occurred following formation of forsterite (Ferry et al., 2011). The single inclusion in sample KP1B with low X^*_{Mg} is an example of how some calcite inclusions in forsterite may equilibrate with the matrix in terms of X^*_{Mg} following entrapment (Ferry, 2001).

Calcite inclusions in garnet in regional metamorphic rocks have the same X^*_{Mg} as calcite in adjacent matrix. Calcite inclusions in garnet, however, can have a different texture than calcite in the matrix. Garnet in sample 21-24C, for example, includes calcite with smaller grain size than calcite in the matrix (Fig. 6b). Five calcite inclusions in each of two garnet grains, as well as matrix calcite adjacent to both garnets, were analyzed for $\delta^{18}O$ in sample 21-24C (Fig. 6b). In addition, five calcite inclusions in one garnet and matrix calcite were analyzed for $\delta^{18}O$ in sample 21-25C. Calcite

inclusions in garnet were analyzed in the two samples to determine if there were differences in $\delta^{18}O$ between inclusion and matrix that correlate with differences in texture.
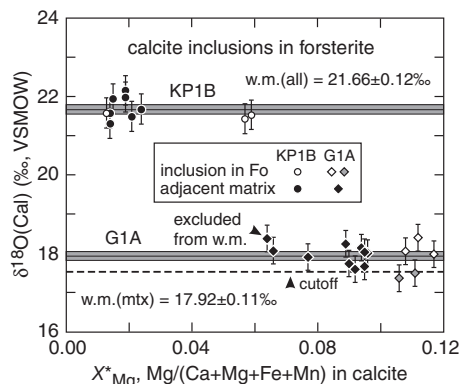

Fig. 7. Measured $\delta^{18}O$ and X^*_{Mg} of calcite inclusions in forsterite (gray and white symbols) and of nearby matrix calcite (black symbols) in contact metamorphosed rocks. Error bars are $\pm 2SD(2)$ of $\delta^{18}O$. The analyses of $\delta^{18}O$ of three calcite inclusions and calcite in nearby matrix in sample KP1B (top) are statistically indistinguishable. The weighted mean (w.m.) of all the calcite analyses is represented by the horizontal line; the gray band is $\pm 2SE$ of the weighted mean. The analyses of $\delta^{18}O$ of matrix calcite in sample G1A (bottom), with a single exception, are statistically indistinguishable. The weighted mean of all analyses of matrix calcite (with the exception of the outlying analysis) is represented by the horizontal black line; the gray band is $\pm 2SE$ of the weighted mean. Two of five analyzed calcite inclusions in forsterite in sample G1A have significantly lower $\delta^{18}O$ than the weighted mean $\delta^{18}O$ of matrix calcite. The dashed horizontal line is the cutoff in $\delta^{18}O$ between inclusion calcite analyses (white diamonds) that are statistically the same as the weighted mean matrix calcite $\delta^{18}O$ and inclusion calcite analyses that are not (gray diamonds).

Results, summarized in Figs. 7 and 8, define two patterns of behavior. One pattern is exhibited by samples KP1B (Fig. 7, top) and 21-24C (Fig. 8a). In both samples the measured $\delta^{18}O$ of calcite inclusions is statistically indistinguishable from the $\delta^{18}O$ of calcite in nearby matrix. There is no correlation between $\delta^{18}O$ and either a difference in X^*_{Mg} between inclusions and matrix grains (sample KP1B) or a difference in grain size between inclusions and matrix grains (sample 21-24C). The second pattern of behavior is exhibited by samples G1A (Fig. 7, bottom) and 21-25C (Fig. 8b). In both cases, all analyses of $\delta^{18}O$ of matrix calcite (21-25C) or all analyses except a single outlier (G1A) are statistically indistinguishable in $\delta^{18}O$ with weighted means as shown in Figs. 7 and 8b. Some analyzed calcite inclusions have $\delta^{18}O$ values that are statistically indistinguishable from those of the matrix grains (open symbols, Figs. 7, 8b) while others do not (gray symbols). The dashed horizontal line in both Figs. 7 and 8b represents the cutoff in $\delta^{18}O$ that separates inclusions that statistically have the same composition as matrix grains and inclusions that do not. In both samples G1A and 21-25C, the inclusions that are statistically different in composition have lower $\delta^{18}O$ than the matrix. Statistically significant differences in $\delta^{18}O$ between inclusions and matrix, however, are small. The two calcite inclusions in sample G1A with the lowest $\delta^{18}O$ are lower than the weighted mean matrix $\delta^{18}O$ by 0.44–$0.57 \pm 0.36‰$ [uncertainty is $\pm 2SD(2)$]. The four calcite inclusions in sample 21-25C with the lowest $\delta^{18}O$ are lower than the weighted mean matrix $\delta^{18}O$ by 0.45–$0.79 \pm 0.35‰$ [$\pm 2SD(2)$].

4.3.2. Quartz inclusions in garnet

Quartz inclusions in garnet also can have a different texture than quartz in the matrix. Garnet in sample 21-24C, for example, includes quartz (as well as calcite) with smaller grain size than quartz (and calcite) in the matrix (Fig. 6b). Quartz and ilmenite inclusions in garnet in sample Q2A
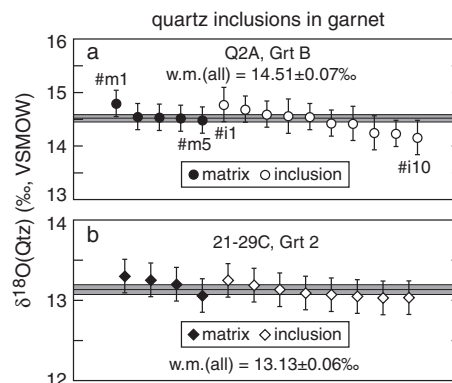

Fig. 8. Measured $\delta^{18}O$ of calcite inclusions in garnet and of nearby matrix calcite in regional metamorphic rocks. Format similar to Fig. 7. (a) Sample 21-24C, garnets A and B. Numbered analyses of matrix calcite, increasing left to right from #m1 to #m5, and of inclusion calcite, increasing from left to right from #i1 to #i5, are the same as numbers of matrix and inclusion calcite in Fig. 6b. All twenty analyses of $\delta^{18}O$ of inclusion and matrix calcite are statistically indistinguishable. (b) 21-25C, garnet A. The $\delta^{18}O$ of four of five analyzed calcite inclusions in garnet A is significantly less than the weighted mean $\delta^{18}O$ (w.m.) of nearby matrix calcite.
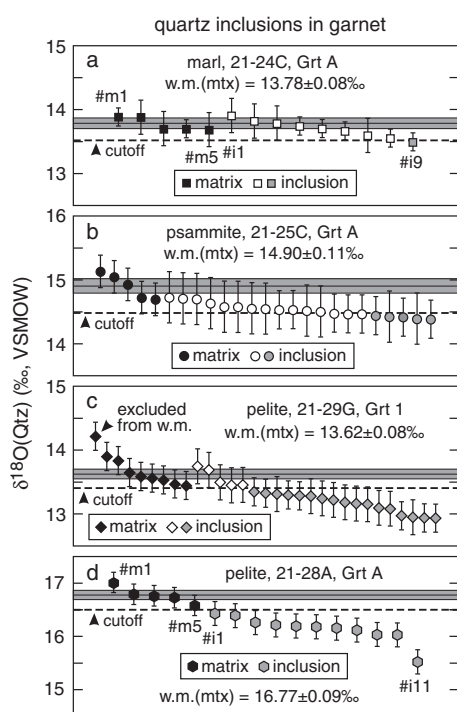

Fig. 9. Measured $\delta^{18}O$ of quartz inclusions in garnet and of nearby matrix quartz in regional metamorphic rocks. Format is the same as in Fig. 8a. All analyses of $\delta^{18}O$ of quartz inclusions and quartz in nearby matrix in each sample are statistically indistinguishable. (a) Sample Q2A, garnet B. Numbers of matrix (#m1 to #m5) and inclusion (#i1 to #i10) quartz analyses are the same as the numbers in Fig. 6c. (b) Sample 21-29C, garnet 2.

define a foliation that occurs at a high angle to foliation in the matrix (Fig. 6c). Quartz inclusions in garnet and quartz in adjacent matrix therefore were analyzed from six samples to determine if inclusion and matrix quartz differed in $\delta^{18}O$ as well.

Results for analyzed quartz inclusions in one representative garnet and nearby matrix quartz in each of the six samples are summarized in Figs. 9 and 10 that have the same format as Fig. 8. The data exhibit the same two patterns of behavior as exhibited by calcite inclusions in garnet (Fig. 8). In samples Q2A and 21-29C (Fig. 9), measured $\delta^{18}O$ of all quartz inclusions is statistically indistinguishable from the $\delta^{18}O$ of quartz in nearby matrix, like the pattern exhibited by calcite in Fig. 8a. There is no correlation

Fig. 10. Measured $\delta^{18}O$ of quartz inclusions in garnet and of nearby matrix quartz in regional metamorphic rocks. Format is the same as in Fig. 8b. In each sample, some or all analyses of $\delta^{18}O$ of quartz inclusions are significantly less than the weighted mean $\delta^{18}O$ (w.m.) of nearby matrix quartz. (a) Sample 21-24C, garnet A. Numbers of matrix (#m1 to #m5) and inclusion (#i1 to #i9) quartz analyses are the same as the numbers in Fig. 6b. The $\delta^{18}O$ analyses of all matrix quartz grains and of all but one quartz inclusion (#i9) are statistically indistinguishable. (b) Sample 21-25C, garnet A. The $\delta^{18}O$ analyses of all matrix quartz and of 15 of 20 analyzed quartz inclusions are statistically indistinguishable. (c) Sample 21-29G, garnet 1. The $\delta^{18}O$ of 17 of 22 analyzed quartz inclusions in garnet is less by a statistically significant margin than the weighted mean $\delta^{18}O$ defined by eight of nine analyses of nearby matrix quartz. (d) Sample 21-28A, garnet A. The $\delta^{18}O$ of all analyzed quartz inclusions in garnet is less by a statistically significant margin than the weighted mean $\delta^{18}O$ of nearby matrix quartz. Numbers of matrix (#m1 to #m5) and inclusion (#i1 to #i11) quartz analyses are the same as the numbers in Fig. 6d.

between $\delta^{18}O$ and a difference in grain size or foliation between inclusions and matrix grains.

In samples 21-24C, 21-25C, 21-29G, and 21-28A (Fig. 10), all analyses of $\delta^{18}O$ of matrix quartz (21-24C, 21-25C, 21-28A) or all analyses except a single outlier (21-29G) are statistically indistinguishable in $\delta^{18}O$ with weighted means as shown in Fig. 10. Like the pattern of calcite inclusions in Fig. 8b, some analyzed quartz inclusions have $\delta^{18}O$ that is statistically indistinguishable from that of the matrix grains (open symbols, Fig. 10) while others do not (gray symbols). In all four samples, the inclusions that are significantly different in composition have lower $\delta^{18}O$ than the matrix. Statistically significant differences in $\delta^{18}O$ between inclusions and matrix, however, are not large. Quartz inclusions in the four samples with measured $\delta^{18}O$ values significantly lower than the weighted mean matrix $\delta^{18}O$ are lower by $0.29 \pm 0.16‰$ (21-24C), $0.43–0.52 \pm 0.32‰$ (21-25C), $0.28–0.69 \pm 0.22‰$ (21-29G), and $0.35–1.26 \pm 0.23‰$ (21-28A) [uncertainty is $\pm 2SD(1)$]. Quartz inclusions in sample 21-28A behave slightly differently than in the other three samples in two regards. First, in sample 21-28A, all analyzed quartz inclusions have $\delta^{18}O$ significantly less than the weighted mean $\delta^{18}O$ of matrix quartz. Second, the difference in $\delta^{18}O$ between one quartz inclusion in sample 21-28A and the weighted mean $\delta^{18}O$ of matrix quartz (1.26‰) is larger than the maximum differences measured in the other three samples (all other differences <0.7‰).

4.3.3. Spatial patterns in the oxygen isotope composition of quartz inclusions in garnet

As with the intracrystalline zoning of minerals in $\delta^{18}O$, a simple and consistent spatial pattern in the $\delta^{18}O$ of quartz inclusions in garnet proved elusive. In garnet A, sample 21-24C (Figs. 6b, 10a), for example, the single quartz inclusion (#i9) that is statistically different in $\delta^{18}O$ from the weighted mean $\delta^{18}O$ of matrix quartz lies midway between the edge and center of the garnet crystal, belying any simple, monotonic, radial trend in the $\delta^{18}O$ of the inclusions. In garnet A, sample 21-28A (Figs. 6d, 10d), the two quartz inclusions that deviate least from the weighted mean $\delta^{18}O$ of matrix quartz (#i1, #i2) and the two that deviate the most (#i10, #i11) all occur close to each other in the interior of the garnet crystal. The quartz inclusion that shows the third least deviation in $\delta^{18}O$ from the weighted mean matrix quartz value (#i3) and the inclusion that exhibits the third greatest deviation (#i9) occur next to each other at the edge of the garnet crystal.

The twenty analyses of $\delta^{18}O$ of quartz inclusions in garnet A, sample 21-25C, were divided between ten inclusions that are intersected by a crack and ten that were unconnected to a crack visible in thin section. There is no simple systematic relation between measured $\delta^{18}O$ of an inclusion and whether it is connected or not to a visible crack. Of fifteen quartz inclusions with $\delta^{18}O$ statistically indistinguishable from the weighted mean value of matrix quartz, eight are connected to a visible crack and seven are not. Of five inclusions that exhibit a statistically significant deviation in $\delta^{18}O$ from the weighted mean matrix value, three are connected to a crack and two are not.

5. OXYGEN ISOTOPE FRACTIONATION BETWEEN COEXISTING MINERAL PAIRS

5.1. Fractionation factors and qualitative analysis

Each sample provided information about the fractionation of oxygen isotopes between one or more mineral pairs with the exception of samples KP1K, 3-4F, 21-29C, and 21-29G for which analyses of only a single mineral are reported. Qualitative and quantitative analysis of the measured fractionations between mineral pairs a and b is based

Table 5
A factors used in analysis of oxygen isotope fractionations between mineral pairs.

Mineral (b)[a]	A(a−b)(K^2)[a]	Reference(s)[b]
quartz	0	
calcite	0.38	1
K-feldspar	0.94	1
plagioclase[c]	$0.94 + 1.03X_{an}$	1
garnet[c]	$2.71 + 0.32 X_{gr}$	2
diopside	2.75	1,3
wollastonite	2.83	1,3,4
kyanite	3.00	1,5
forsterite	3.67	1,3
kyanite	0.70A(quartz-garnet)	6

[a] A(a-b)$(10^6/T^2) = 1000\ln\alpha$(a–b), all referenced to a = quartz.
[b] References: 1 = Clayton et al. (1989); 2 = Valley et al. (2003); 3 = Chiba et al. (1989); 4 = Matthews et al. (1983); 5 = Tennie et al. (1998); 6 = Sharp (1995).
[c] X_{an} = mole fraction anorthite component; X_{gr} = mole fraction grossular component.

on the relation $1000\ln\alpha$(a–b) $= A$(a–b)$(10^6/T^2)$ with all A terms referenced to a = quartz and T is in K (Table 5). Values of A that pair quartz with calcite, feldspar, diopside, and forsterite are from Chiba et al. (1989) and Clayton et al. (1989). Additional A values are based on results of laboratory experiments by others involving wollastonite and kyanite (Table 5). Oxygen isotope fractionation between quartz and K-feldspar was considered the same as between quartz and albite. Quartz-garnet oxygen isotope fractionations depend on garnet composition (Keiffer, 1982; Rosenbaum and Mattey, 1995; Kohn and Valley, 1998; Valley et al., 2003). Following the review of Valley et al. (2003), A(quartz-garnet) was taken as linear function of X_{gr}, the mole fraction of the grossular component (Table 5). For reasons that will be clear in Section 5.2, the calibration of quartz-kyanite fractionation, based on Sharp's (1995) analysis of naturally occurring mineral pairs, was also considered. Fractionations involving dolomite are poorly known and were ignored.

The calibrations of fractionation in Table 5 predict that at equilibrium, regardless of T, δ^{18}O of coexisting minerals should decrease in the order: quartz > calcite > K-feldspar > plagioclase > almandine > diopside ≥ wollastonite > grossular > forsterite. The δ^{18}O of kyanite is predicted to be less than that of wollastonite and greater than that of grossular (Tennie et al., 1998, calibration) or greater than almandine and less than plagioclase with $X_{an} < 0.93$ (Sharp, 1995, calibration). Surprisingly, with one exception, in spite of the large grain-to-grain variations in δ^{18}O of many minerals, data in Figs. 3 and 4 do not document any statistically significant reverse fractionations between coexisting mineral pairs with reference to this order. Either mineral pairs exhibit the qualitatively
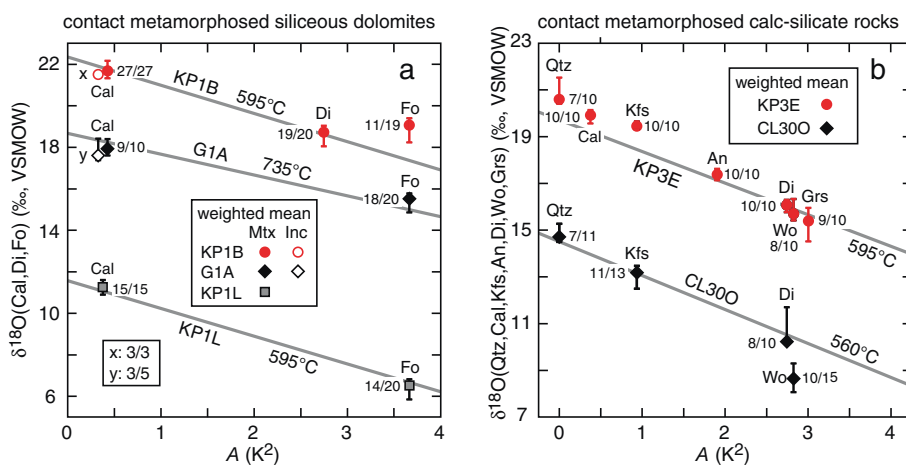

Fig. 11. Quantitative analysis of oxygen isotope fractionation between all analyzed mineral pairs in contact metamorphosed rocks. The value of A is defined by the equation $1000\ln\alpha$(a-b) $= A$(a–b)$(10^6/T^2)$, with a = quartz (Table 5) and T is in K. Except for garnet, vertical lines represent the total range of measured δ^{18}O of each mineral in a sample. Because of the larger uncertainty in bias*(garnet) compared to corresponding terms for other minerals, vertical lines for garnet represent the range in measured values augmented by ±2SD(2). The weighted mean δ^{18}O of the largest group of analyses of a given mineral that are statistically indistinguishable is represented by symbols (black, gray, or colored for matrix grains; white for inclusions). The size of the symbols is approximately ±2SE of the weighted mean (Table 2) or slightly larger depending on the scale of the δ^{18}O axis. The denominator of each fraction is the total number of analyses of each mineral in a sample; the numerator is the number of these analyses that are statistically indistinguishable and that were used to calculate the weighted mean. For clarity, the A values for inclusion-matrix pairs have been separated by ±0.05 relative to their correct plotting position. Gray lines are isotherms defined by the T of mineral equilibrium (Table 1). (a) Siliceous dolomite marbles. (b) Calc-silicate rocks.

expected fractionation or the $\delta^{18}O$ values of mineral pairs are statistically indistinguishable (e.g., forsterite and diopside in sample KP1B, Fig. 3b). The exception is the positive kyanite-garnet fractionation of 1–2‰ in samples E6 and Gass (Table 2; Fig. 4c) that are inconsistent with A(quartz-kyanite) in Table 5 based on the experiments of (Tennie et al., 1998) [but consistent with the calibration of A(quartz-kyanite) by Sharp (1995)].

5.2. Quantitative analysis of fractionations on A–δ diagrams

Fractionations between all coexisting mineral pairs were evaluated quantitatively using A–δ diagrams (Javoy et al., 1970), where δ is the measured $\delta^{18}O$ of each mineral in a sample and the A values are those in Table 5. Considering that normally at least ten measurements were made of $\delta^{18}O$ of each mineral in each sample, there is uncertainty about what to plot as the value of δ. Accordingly, the value of $\delta^{18}O$ for each mineral is represented on A–δ diagrams in two ways. The first is to plot the total range in $\delta^{18}O$ measured for a given mineral in a sample. The second is to plot the weighted

mean of the largest group of analyses that are statistically consistent with a single value (employing the same criterion used to judge grain-to-grain and intracrystalline homogeneity of minerals in $\delta^{18}O$ in Section 4.1.1. and type 2 SDs for all minerals). The weighted mean of this group is listed in Table 2 for each analyzed mineral. In the case of homogeneous minerals, the weighted mean is the best estimate of the $\delta^{18}O$ for a given mineral in a sample.

Because of the very large variability in $\delta^{18}O$ of forsterite and calcite in samples B1W and B43A (Fig. 3), quantitative consideration of mineral fractionations in the two samples makes no sense. Results for all other samples are presented in Fig. 11 for contact metamorphic rocks and in Fig. 12 for regional metamorphic rocks. Contact metamorphic rocks in Fig. 11 are further divided by lithology. Regional metamorphic rocks in Fig. 12 are further divided by lithology, and in the case of pelites, by grade of metamorphism. Gray inclined lines on the A-δ diagrams are isotherms whose slopes are defined by the inferred T of mineral equilibrium in each sample, taken from earlier publications (Table 1). Higher temperature isotherms have shallower slopes; the
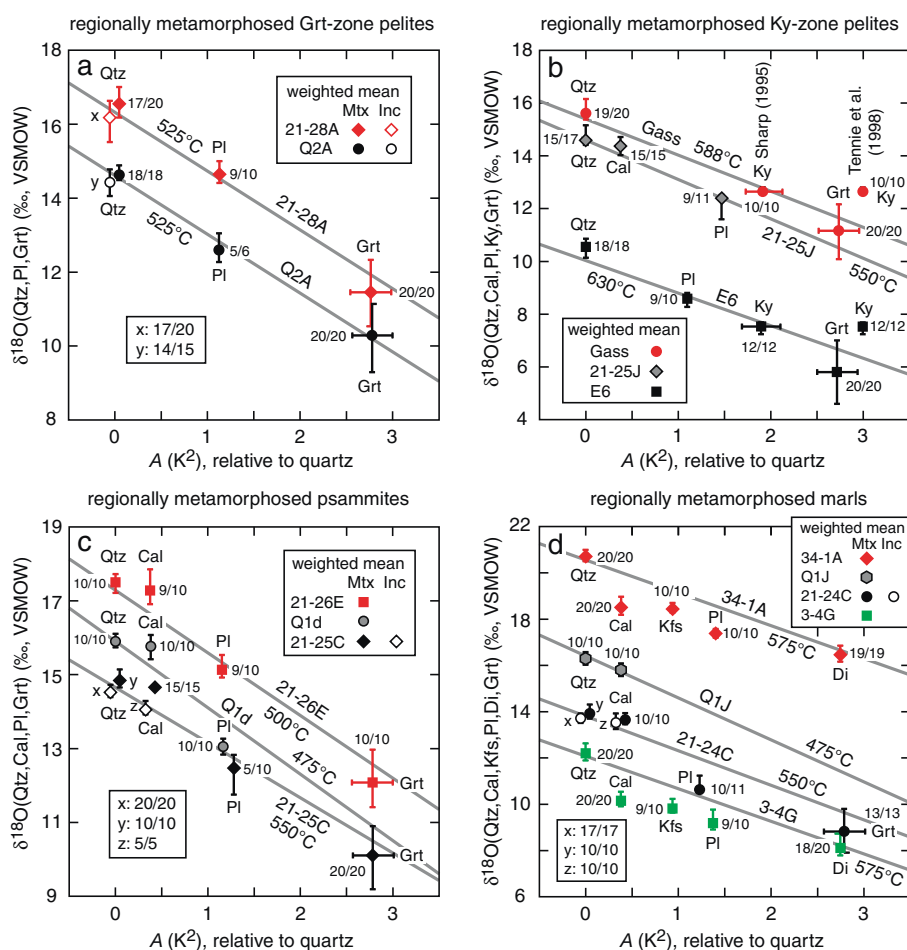

Fig. 12. Quantitative analysis of oxygen isotope fractionation between all analyzed mineral pairs in regional metamorphed rocks. Formats are the same as Fig. 11. Horizontal lines illustrate the uncertainties in A(quartz-garnet) and A(quartz-kyanite) derived from the uncertainties in A(quartz-zircon) and A(zircon-almandine) in Valley et al. (2003) and the uncertainty in the factor that relates A(quartz-kyanite) to A(quartz-garnet) in Sharp (1995). (a) Pelites from the garnet zone. (b) Pelites from the kyanite zone. Two values of A(quartz-kyanite) are shown (Table 5). (c) Psammites. (d) Marls.

δ intercepts are controlled by $\delta^{18}O$ of the minerals. Each isotherm was initially positioned along the $\delta^{18}O$ axis by eye to intersect as many of the measured ranges in $\delta^{18}O$ in a given sample as possible and then further adjusted to pass as close to as many of the weighted mean values of $\delta^{18}O$ of matrix grains as possible.

None of the equilibrium isotherms pass through the $\pm2SE$ interval about the weighted mean $\delta^{18}O$ values for all analyzed minerals in the corresponding sample. The samples in Figs. 11 and 12 were assigned to one of two groups based on the ranges of measured $\delta^{18}O$ values. The two groups highlight the different degree to which minerals in the seventeen samples attained and preserved oxygen isotope exchange equilibrium at the inferred T of mineral equilibrium. The groupings transcend considerations of lithology or of the environment or grade of metamorphism. Both contact and regional metamorphic rocks are represented in both groups. Among regional metamorphic rocks, both groups contain samples from the biotite, garnet, and kyanite zones, and both groups contain pelites, psammites, and marls. Specifically, the first group consists of samples KP1L and G1A (Fig. 11a), Q2A and 21-28A (Fig. 12a), Gass and 21-25J (Fig. 12b), and Q1J (Fig. 12d). The isotherm for each of the seven samples passes through the range in measured $\delta^{18}O$ [or range $\pm2SD(2)$ in the case of garnet]. The weighted mean $\delta^{18}O$ of each analyzed mineral in the first group deviates from its isotherm by no more than 0.7‰. There is no difference in the behavior of matrix grains and inclusions of the same mineral in samples G1A, Q2A, and 21-28A. The seven samples represent rocks in which all analyzed minerals approached and preserved oxygen isotope exchange equilibrium with each other well enough that the range in measured $\delta^{18}O$ of every analyzed mineral is consistent, within error of measurement, with the inferred T of mineral equilibrium. The conclusion for a close approach to isotopic equilibrium between kyanite and the other analyzed minerals in sample Gass holds only if the A(quartz-kyanite) value is based on the calibration of Sharp (1995) rather than on the laboratory experiments of Tennie et al. (1998).

The second group is composed of samples KP1B (Fig. 11a); KP3E and CL30O (Fig. 11b); E6 (Fig. 12b); 21-26E, Q1d, and 21-25C (Fig. 12c); and 34-1A, 24-24C, and 3-4G (Fig. 12d). Samples in the second group are distinguished from those in the first by containing one or more minerals whose range in measured $\delta^{18}O$ does not intersect the isotherm of inferred mineral equilibrium. Specifically, these include forsterite and inclusion calcite in sample KP1B; quartz, calcite, and K-feldspar in sample KP3E; wollastonite in sample CL30O; quartz in sample E6; calcite and plagioclase in sample Q1d; calcite in sample 21-26E; matrix calcite in sample 21-25C; calcite, K-feldspar, and plagioclase in both samples 34-1A and 3-4G; and matrix calcite and plagioclase in sample 21-24C. The weighted mean $\delta^{18}O$ of some analyzed minerals in the second group may deviate from their isotherm by up to 1.7‰ (e.g., forsterite in sample KP1B; wollastonite in sample CL30O). In spite of the disequilibrium exhibited by one or more minerals in these samples, two or more other minerals in each sample have weighted mean $\delta^{18}O$ values that deviate from

the isotherm by $\leqslant0.3$‰ (with the exception of sample Q1d). The better equilibrated minerals are diopside and matrix calcite in sample KP1B; anorthite, diopside, wollastonite, and grossular in sample KP3E; quartz, K-feldspar, and diopside in sample CL30O; plagioclase and kyanite in sample E6; quartz and plagioclase in sample 21-26E; matrix and inclusion quartz, inclusion calcite, and plagioclase in sample 21-25C; quartz and diopside in samples 34-1A and 3-4G; and matrix and inclusion quartz and inclusion calcite in sample 21-24C. Except sample Q1d, Group 2 samples thus are a mix of at least two analyzed minerals that closely approached and preserved oxygen isotope exchange equilibrium at the inferred T of mineral equilibrium and at least one mineral whose $\delta^{18}O$ deviates significantly from equilibrium at that T.

As with sample Gass, the range in measured $\delta^{18}O$ of kyanite in sample E6 (Fig. 12b) would also miss intersection with the isotherm if the A(quartz-kyanite) value is based on the laboratory experiments of Tennie et al. (1998) rather than on the calibration of Sharp (1995). In addition, the observed positive kyanite-garnet oxygen isotope fractionation in the two samples does not match that predicted by the experiments of Tennie et al. (1998). Results of this study support the conclusion of Putlitz et al. (2002) that the empirical A(quartz-kyanite) factor of Sharp (1995) is preferred over one based on the experiments of Tennie et al. (1998).

With the exception of garnet in sample Q2A, the weighted mean $\delta^{18}O$ of garnets in Fig. 12 consistently falls below the isotherms based on mineral equilibria by 0.4–0.9‰. It is uncertain the degree to which the mismatch is explained by error in bias*(garnet) (see Appendix A), by a value of A(quartz-garnet) that is too low (but within the range of values in Fig. 12 consistent with the calibration of Valley et al., 2003), by systematic oxygen isotope exchange disequilibrium between garnet and most other minerals in the samples, or by some combination of these factors. Modification of $\delta^{18}O$ of garnet following initial crystallization seems an unlikely explanation both because oxygen diffusion in garnet is probably very slow (Martin et al., 2011, 2014; Page et al., 2014) and because garnet typically exhibits no textural evidence for recrystallization after it formed (e.g., Fig. 6).

6. DISCUSSION

6.1. Departures from grain-scale oxygen isotope exchange equilibrium

Grain-scale oxygen isotope exchange disequilibrium is common in both contact and regional metamorphic rocks, and it takes several different forms. First, different grains of the same mineral separated by a few 100 μm or less can have significantly different $\delta^{18}O$ (e.g., Fig. 2a). Second, there can be significant variations in $\delta^{18}O$ within an individual mineral crystal (e.g., Figs. 2 and 5). Third, there can be significant differences in $\delta^{18}O$ between the occurrence of minerals in the matrix and their occurrence as inclusions in other minerals in the same sample (e.g., Figs. 7, 8 and 10). Fourth, coexisting mineral pairs in a sample can exhibit

non-equilibrium oxygen isotope fractionations (e.g., Figs. 11 and 12). A variety of phenomena can explain the observed departures from isotope equilibrium at the grain-size scale.

6.1.1. Overstepped metamorphic mineral reactions

The degree of both grain-to-grain and intracrystalline variation in $\delta^{18}O$ of forsterite in marbles (Fig. 13) is positively correlated with forsterite crystal number density (number of crystals per cm^3). Crystal number density of a product mineral, in turn, is positively correlated with nucleation rate and hence degree of overstepping the reaction that produced that mineral (Ridley and Thompson, 1986; Roselle et al., 1997; Müller et al., 2004; Ferry et al., 2011). One process therefore that explains departures from oxygen isotope exchange equilibrium in samples from this study is overstepping of metamorphic mineral reactions. The effect is pronounced in forsterite marbles because forsterite was produced by an infiltration-driven reaction in which the fluid was initially far from equilibrium with the rock it infiltrated (Ferry et al., 2011). Wollastonite in sample CL30O was also produced by an infiltration-driven reaction (Ferry et al., 2001). A large departure from mineral-fluid equilibrium during the wollastonite-forming reaction therefore likewise may explain both the variability in $\delta^{18}O$ of wollastonite in the sample and its large departure from isotope exchange equilibrium with coexisting minerals (Fig. 11b). The microscopic mechanism by which large departures from mineral-fluid equilibrium during reaction cause highly variable $\delta^{18}O$ of product minerals, however, is not understood.

6.1.2. Growth zoning

The $\delta^{18}O$ values of minerals in a rock change during metamorphic mineral reactions because of the fractionation of oxygen isotopes among reactants and products (Rumble, 1982). If oxygen diffusivity in a product mineral is low, the change in $\delta^{18}O$ can be preserved as systematic intracrystalline zoning in $\delta^{18}O$ (Kohn, 1993; Kohn et al., 1993). When a product mineral has the lowest or one of the lowest $\delta^{18}O$ of all minerals in a rock, the predicted zonation pattern for prograde heating is from lower $\delta^{18}O$ in the core to higher $\delta^{18}O$ at the rim (Kohn, 1993). Examples of product minerals in this study that are both low in $\delta^{18}O$ compared to coexisting minerals and have low oxygen diffusivity include diopside, garnet, forsterite, and probably wollastonite (Figs. 11 and 12; Cole and Chakraborty, 2001, their Fig. 23a). Isotopically zoned diopside commonly exhibits an increase in $\delta^{18}O$ from interior to edge (Fig. 5c, Table 4C), as does wollastonite in sample KP3E (Table 4C). Oxygen isotope zonation in forsterite, however, is not systematic (Fig. 2), and it is difficult to determine to what degree observed zonation is due to growth or to a large departure from mineral-fluid equilibrium during reaction (Fig. 13). No significant growth zoning in $\delta^{18}O$ in garnet was detected in this study, in part, because of the relatively large uncertainty in measured $\delta^{18}O$ values introduced by uncertainties in values of *bias**(garnet).

6.1.3. Isotope transport at or near the peak of metamorphism

Oxygen isotope exchange disequilibrium in the form of large variations in $\delta^{18}O$ within individual grains can result from transport of isotopes either by fluid flow (i.e., infiltration) or by diffusion at or near the peak of metamorphism. The best example of isotope disequilibrium caused by fluid flow is in sample KP1L. The sample is composed of dolomite marble cut by a forsterite-calcite vein produced by infiltration and silicification of dolomite by a CO_2-poor, Si-bearing, low-$\delta^{18}O$ aqueous fluid at the peak of metamorphism (Ferry et al., 2011). Forsterite and calcite have $\delta^{18}O$ ($\sim$6–7‰, $\sim$11–12‰, respectively, Table 2A) that is significantly less than that of dolomite distal from the vein ($\sim$19–20‰, Table 2A). Isotope transport from vein fluid to adjacent grains of dolomite produced large intracrystalline variations in $\delta^{18}O$, with values in the range $\sim$9–19‰ (Fig. 5a). The contrast between isotopically altered low-$\delta^{18}O$ dolomite and unaltered dolomite over a distance of 10–20 μm within a single grain and the absence of a coherent spatial pattern to the measured $\delta^{18}O$ values within the grain with reference to the grain's contact with the vein (Fig. 5a) both suggest that the mechanism of alteration was solution and reprecipitation of dolomite rather than solid-state diffusion.

Of 232 grains examined, the best example in this study of intracrystalline oxygen isotope disequilibrium caused by diffusion-controlled isotope transport is a quartz grain in sample CL30O that is smoothly zoned in $\delta^{18}O$ over a distance of $\sim$200 μm from a value of 14.2‰ in the interior to 15.4‰ at the edge (Fig. 5d). The zoning cannot be growth zoning because quartz is a reactant in the principal prograde metamorphic reaction experienced by the sample (Ferry et al., 2001).

In both the case of the dolomite grain in sample KP1L and the quartz grain in sample CL30O, cooling following isotope transport must have been rapid enough to prevent diffusion from erasing the intracrystalline variability in $\delta^{18}O$ (Eiler et al., 1992, 1993; Valley, 2001).
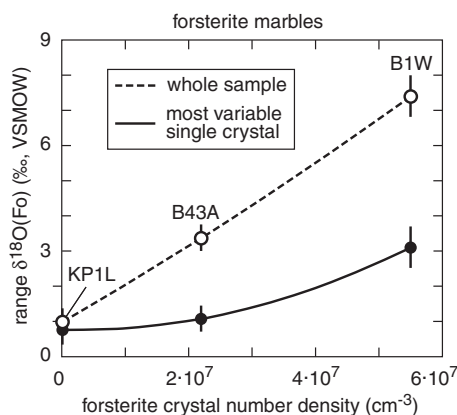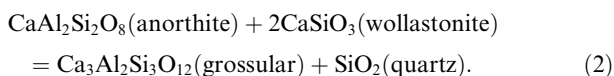

Fig. 13. The crystal number density (number forsterite crystals per cm^3 rock) and measured intercrystalline and intracrystalline range in $\delta^{18}O$ of forsterite in three samples of contact metamorphosed siliceous dolomite marble. Ranges in $\delta^{18}O$ from this study and Ferry et al. (2010). Values of crystal number density from Ferry et al. (2011).

6.1.4. Retrograde mineral reactions

If a mineral forms during cooling, it may have a $\delta^{18}O$ value that is inconsistent with equilibrium with coexisting prograde minerals at the peak T of metamorphism, particularly if there is a large isotope fractionation between the retrograde and peak minerals. A likely example is quartz in sample KP3E that occurs as amoeboid aggregates that appear to have developed along grain boundaries between peak minerals like wollastonite, K-feldspar, and calcite (Fig. 14). Grossular nearby also appears to have formed as a thin film along grain boundaries (Fig. 14). Textures illustrated in Fig. 14 imply that formation of quartz and grossular developed at the expense of wollastonite and anorthite following peak metamorphism by the retrograde reaction,

$$CaAl_2Si_2O_8(\text{anorthite}) + 2CaSiO_3(\text{wollastonite})$$
$$= Ca_3Al_2Si_3O_{12}(\text{grossular}) + SiO_2(\text{quartz}). \qquad (2)$$

(The proportions of grossular and quartz in Fig. 14 are not representative of sample KP3E as a whole that contains more grossular than quartz). Because of the large oxygen isotope fractionations between quartz and the other principal minerals in the rock (wollastonite and diopside), $\delta^{18}O$ of quartz formed at lower T (below that defined by equilibrium between diopside and wollastonite) should lie above the isotherm in Fig. 11b, as is observed. The $\delta^{18}O$ of grossular does not significantly deviate from the isotherm for sample KP3E because oxygen isotope fractionations among grossular, wollastonite, and diopside are small.

6.1.5. Oxygen isotope exchange among minerals and fluid during cooling

Minerals continue to exchange oxygen isotopes with other coexisting minerals as rocks cool. Minerals most affected are those with high oxygen diffusivity such as calcite and fe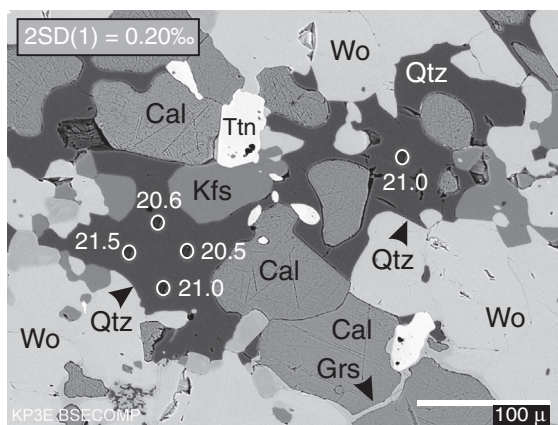ldspar; minerals least affected are those with low oxygen diffusivity such as garnet, diopside, and probably wollastonite. Quartz likely exhibits intermediate behavior. Closed system exchange will occur if there is little or no fluid present during cooling. Possible examples are calcite and plagioclase in regionally metamorphosed psammite samples Q1d and 21-25C (Fig. 12c) and one marl sample from the Gile Mountain Formation (sample 21-24C, Fig. 12d). Matrix calcite in all three samples has $\delta^{18}O$ that lies above the isotherm that passes close to coexisting quartz while plagioclase has $\delta^{18}O$ that lies below the isotherm (Fig. 12c and d). Because the calcite-plagioclase oxygen isotope fractionation is positive, the deviations could be explained by isotope exchange between the two minerals as the rocks cooled. The lower oxygen diffusivity in quartz (Cole and Chakraborty, 2001, their Fig. 23a) explains why $\delta^{18}O$ of quartz was little affected, if at all.

Open-system exchange will occur if fluid continues to flow through rocks as they cool and minerals exchange oxygen isotopes with the fluid. Possible examples include regionally metamorphosed marls from the Waits River Formation (samples 34-1A and 3-4G, Fig. 12d) and contact metamorphosed calc-silicate marble, sample KP3E (Fig. 11b). Calcite, K-feldspar, and plagioclase in the regionally metamorphosed marls all have $\delta^{18}O$ values that lie below the mineral equilibrium isotherm consistent with the $\delta^{18}O$ of coexisting quartz and diopside. The reduced value of $\delta^{18}O$ of the three minerals relative to the isotherm could be explained by isotope exchange during cooling with a relatively low-$\delta^{18}O$ fluid. The elevated $\delta^{18}O$ of calcite and K-feldspar in sample KP3E, relative to the isotherm consistent with the $\delta^{18}O$ of diopside and wollastonite, implies exchange of calcite and feldspar with a relatively high-$\delta^{18}O$ fluid. The lower oxygen diffusivity in quartz and diopside (Cole and Chakraborty, 2001, their Fig. 23a) explains why $\delta^{18}O$ of quartz in samples 34-1A and 3-4G and of diopside in all three samples was little affected, if at all.

Differences in $\delta^{18}O$ between inclusions and matrix grains of calcite and quartz (Figs. 7, 8 and 10) likewise can be explained by oxygen isotope exchange among matrix minerals as rocks cooled. Where significant differences in $\delta^{18}O$ are present, $\delta^{18}O$ of inclusions is always less than that of grains of the same mineral in the matrix. At isotope exchange equilibrium, $\delta^{18}O$ of quartz and calcite is greater than that of other coexisting minerals. Isotope exchange among matrix minerals during cooling therefore increases the $\delta^{18}O$ of quartz and calcite at the expense of other minerals. Grains of quartz and calcite, trapped as inclusions in forsterite or garnet during prograde mineral growth and then isolated from isotope exchange with matrix grains, would preserve the initially lower values of $\delta^{18}O$, as observed. The $\delta^{18}O$ of 80% of analyzed calcite inclusions trapped in a garnet in sample 21-25C is lower than $\delta^{18}O$ of calcite grains in the matrix by a statistically significant margin (Fig. 8b). In contrast, $\delta^{18}O$ of only 25% of the quartz inclusions in the same garnet is significantly lower than $\delta^{18}O$ of matrix quartz (Fig. 10b). The observation implies that oxygen isotope exchange between matrix quartz and other matrix minerals effectively stopped at a higher T during cooling than did isotope exchange between matrix calcite and other matrix minerals.

Fig. 14. BSE image of a region in sample KP3E showing the petrographic context of analyzed quartz and measured values of $\delta^{18}O$ (‰, VSMOW). Analysis pits are the same size and location as the white ovals. The textures of quartz (Qtz) and grossular (Grs) suggest that they developed along grain boundaries during retrograde metamorphism after the crystallization of wollastonite (Wo), calcite (Cal), and K-feldspar (Kfs). Ttn is titanite.

6.1.6. Time versus temperature of metamorphism

The T of metamorphism alone does not appear to be a primary factor in controlling the intercrystalline and intracrystalline variability in $\delta^{18}O$ in metamorphic rocks in this study. For example, all analyzed minerals in regionally metamorphosed samples Q1d and Q1J, that experienced peak T of metamorphism ~475 °C, exhibit no detectable grain-to-grain variability or zoning in $\delta^{18}O$ (Table 2B). In contrast, there is significant intercrystalline and intracrystalline variability in $\delta^{18}O$ in both forsterite and calcite in samples B1W and B43A that experienced peak T of contact metamorphism ~200 °C higher (Tables 1A, 2A, Figs. 2 and 3). In addition, there is no systematic decrease in the degree of grain-to-grain variability or zoning in $\delta^{18}O$ in minerals in regional metamorphic rocks with increasing grade of metamorphism (2B, 4B; Fig. 4). The principal difference in variability in $\delta^{18}O$ found in this study is between more variable minerals in contact metamorphic rocks like samples B1W and B43A and less variable minerals in regional metamorphic rocks like samples Q1d and Q1J (Figs. 3 and 4). Peak T either overlaps or is higher in the analyzed samples of contact metamorphic rock than in the analyzed samples of regional metamorphic rock (Table 1). The explanation for the difference in behavior is the much longer duration of regional than of contact metamorphism. Among the samples examined in this study, the longer duration of regional metamorphism appears to have dominated over the generally higher peak temperatures attained during contact metamorphism in controlling the degree to which grain-scale oxygen isotope exchange equilibrium was attained during metamorphism. Sections 6.1.1.–6.1.5., of course, identify other factors besides time and temperature that are important as well.

6.2. Duration of metamorphic process from intracrystalline diffusion profiles

Measured oxygen isotope profiles in zoned mineral grains potentially can provide quantitative constraints on the duration of metamorphic processes. An example is the $\delta^{18}O$ profile in a single quartz grain from sample CL30O from the Mt. Morrison pendant (Fig. 5d). Following Crank (1975), the data in Fig. 5d have been replotted in Fig. 15 in terms of dimensionless distance and dimensionless oxygen isotope composition. With the exception of the single datum at $d/r = 0.46$, the profile is consistent with diffusion between a spherical quartz grain with an initially uniform $\delta^{18}O = \delta^{18}O_0 = 14.2\%$ and a surrounding reservoir whose $\delta^{18}O$ is fixed at equilibrium with quartz with $\delta^{18}O = \delta^{18}O_1 = 15.5\%$ (Fig. 15). Most data cluster around a value of $Dt/r^2 \approx 0.02$, where D is the diffusion coefficient for oxygen in quartz, t is the duration over which the profile developed, and r is the radius of the quartz grain. The approximately constant value of Dt/r^2 indicates that the different $\delta^{18}O$ analyses of the quartz grain in Fig. 5d are consistent with a single duration of diffusion, or nearly so.

Constraints on the duration of metamorphic processes follow from a choice of the value of D. Three processes are evaluated using the experimental determination of oxygen diffusion in quartz by Giletti and Yund (1984) under
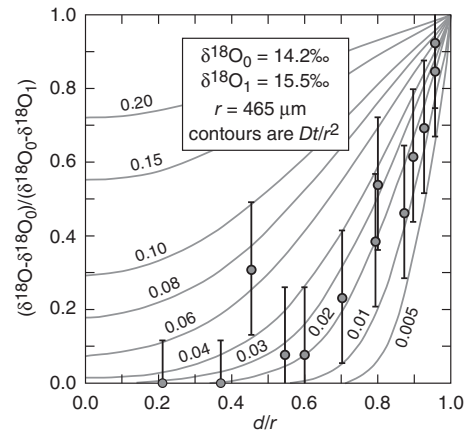

Fig. 15. Plot of dimensionless oxygen isotope composition against dimensionless distance (Fig. 4.1 of Crank, 1975). Contours of Dt/r^2 refer to oxygen diffusion between a sphere with initially uniform $\delta^{18}O_0$ and a surrounding reservoir with fixed $\delta^{18}O_1$; D is the diffusion coefficient of oxygen in quartz, r is the radius of the sphere, t is the duration of diffusion, and d is radial distance from the center of the sphere. Data points are based on values of d, r, $\delta^{18}O_0$, and $\delta^{18}O_1$ for the quartz grain in sample CL30O illustrated in Fig. 5d, recast in dimensionless variables. Error bars correspond to ±2SD(1). All data (except the datum at $d/r = 0.46$) cluster about a value of $Dt/r^2 \approx 0.02$. The outlying datum at $d/r = 0.46$ is identified by the red value of $\delta^{18}O$ in Fig. 5d.

hydrothermal conditions at 1 kbar and 500–550 °C with diffusion parallel to the c axis. Experimental conditions are similar to those during infiltration-driven contact metamorphism in the Mt. Morrison pendant (Table 1), and oxygen diffusion in quartz exhibits only a small dependence on crystallographic orientation (Giletti and Yund, 1984). First, an upper bound on the grain's residence time at the T recorded by mineral equilibria was computed from $Dt/r^2 = 0.02$ and $D = 2.94 \cdot 10^{-16}$ cm^2/s at 560 °C; $t = 4650$ y. It is a maximum time because the calculation ignores the duration of heating and cooling during contact metamorphism. Second, an upper bound on the duration of linear cooling between 560 °C and some low value such as 200 °C at which significant oxygen diffusion in quartz ceases was calculated from $\overline{D}\, t/r^2 = 0.02$ with $\overline{D}$ the effective value of D during cooling, computed from:

$$\overline{D} = \left[\int_{200}^{560} D(T)dT \right]/360 = 1.63 \cdot 10^{-17}\, \text{cm}^2/\text{s} \qquad (3)$$

(the exact lower limit of integration is unimportant). The calculated duration of 83,900 y is a maximum value because the duration of heating to 560 °C is ignored. Third, the duration of linear heating from 200 to 560 °C, immediately followed by linear cooling back to 200 °C, for $\overline{D}\, t/r^2 = 0.02$, is also 83,900 y because the effects of linear heating and cooling are identical. Calculated values of t scale linearly with $\overline{D}\, t/r^2$; if $\overline{D}\, t/r^2 = 0.04$ or 0.01, for example, all calculated times would be larger or smaller by a factor of two. Calculated durations of oxygen isotope diffusion during cooling or during heating and cooling are consistent with those predicted from conductive thermal models of contact metamorphism (Nabelek et al., 2012). The inferred short

residence time at peak T is consistent with durations of infiltration-driven metamorphism predicted by coupled thermal-hydrologic models (Cook et al., 1997). Calculated times are meaningful, however, only to the extent that assumptions used in computing the contours in Fig. 15 are valid.

6.3. Textures and the oxygen isotope geochemistry of metamorphic rocks

Grain scale analysis of minerals for $\delta^{18}O$ allows for integration of oxygen isotope transport during metamorphism with the development of textures. Several examples are reviewed. The extreme intracrystalline variability of $\delta^{18}O$ in dolomite in sample KP1L (Fig. 5a) was recognized by Ferry et al. (2010). They postulated that infiltration of low-$\delta^{18}O$ fluid into dolomite occurred along healed fractures visible in thin section as zones of turbidity. Turbidity is preferentially developed along gently curved bands that cut across dolomite grains (black arrow, Fig. 5a), along cleavage (white arrow, Fig. 5a), and along some grain boundaries (black arrows, Fig. 5b). There is no correlation, however, between $\delta^{18}O$ and the occurrence or absence of turbidity. In sample KP1L values of $\delta^{18}O$ in the ranges 9–11‰ and 18–19‰ occur in both turbid and limpid dolomite (Fig. 5a). In related sample KP1K, a dolomite marble from the same outcrop, dolomite has been altered to $\delta^{18}O$ values in the range 4.5–5.5‰ (Fig. 5b). Turbid and limpid dolomite exhibit no significant difference in $\delta^{18}O$. Turbidity is caused by a myriad of decrepitated fluid inclusions. Zones of turbid dolomite in both samples therefore directly image grain-scale pathways along which at some point in the rocks' histories there was focused fluid flow along fractures, cleavage, and grain boundaries. The pathways imaged by turbidity, however, are not those exclusively followed by low-$\delta^{18}O$ fluids responsible for the ^{18}O-depletion in dolomite. Imaging of the dolomite grain in sample KP1L with highly variable $\delta^{18}O$ by cathodoluminescence (Fig. 5e) fails, as well, to reveal the spatial pattern of infiltration of the low-$\delta^{18}O$ fluids.

Matrix calcite in sample G1A has lower X^*_{Mg} than many calcite inclusions in forsterite (Fig. 6a) because dolomite has exsolved from matrix calcite during cooling but not from most inclusion calcite (Ferry, 2001). Many irregularly shaped dolomite grains produced by exsolution are visible in Fig. 6a. The difference in $\delta^{18}O$ between inclusion and matrix calcite (Fig. 7), however, is either statistically insignificant or small, 0.44–0.57 ± 0.36‰ [±2SD(2)]. Dolomite exsolution from calcite during cooling of sample G1A evidently had little or no effect on $\delta^{18}O$ of calcite.

Quartz and calcite inclusions in garnet in sample 21-24C define a finer-grained texture at the time of garnet growth than the texture preserved in the matrix (Fig. 6b). The $\delta^{18}O$ of inclusions of calcite and quartz in garnet and of calcite and quartz in nearby matrix is either statistically indistinguishable (calcite, Fig. 8a) or statistically indistinguishable with the exception of a single analyzed inclusion (quartz, Fig. 10a). Quartz inclusions in garnet in sample Q2A define a foliation at the time of garnet growth that differed from the foliation displayed in the matrix (Fig. 6c). The $\delta^{18}O$ of quartz

inclusions in garnet and of quartz in nearby matrix is statistically indistinguishable (Fig. 9a). In both samples 21-24C and Q2A, significant changes in the texture of the matrix of the rocks following garnet growth apparently were not associated with any measurable change in the $\delta^{18}O$ of matrix quartz or matrix calcite. The conclusion, however, is subject to qualifications that follow.

The $\delta^{18}O$ of quartz inclusions in garnet may or may not differ significantly from the $\delta^{18}O$ of quartz in adjacent matrix grains (Figs. 9 and 10). There is a qualitative correlation between the number and density of quartz inclusions in garnet and whether the $\delta^{18}O$ of quartz inclusions and nearby matrix quartz grains are statistically the same or different. Garnets that are choked with numerous, large quartz inclusions contain quartz inclusions that have $\delta^{18}O$ that is statistically indistinguishable from the $\delta^{18}O$ of matrix grains or indistinguishable with a single exception (e.g., samples 21-24C and Q2A; Figs. 6b,c, 9a, 10a). In garnets that contain few, small quartz inclusions, all analyzed quartz inclusions have $\delta^{18}O$ that is lower than the $\delta^{18}O$ of matrix grains by a statistically significant margin (e.g., sample 21-28A; Figs. 6d, 10d). The correlation, in turn, suggests a textural control on the degree to which quartz inclusions in garnet and adjacent matrix quartz grains differ in $\delta^{18}O$. When quartz inclusions are large and numerous (Fig. 6b and c), cracks will develop during cooling because of the substantial difference in thermal expansion between quartz and garnet (~40% relative, Holland and Powell, 1990). The cracks then can serve as pathways along which oxygen isotope exchange between inclusion and matrix grains can continue after entrapment of the inclusions. When quartz inclusions are smaller and less abundant (Fig. 6d), cracking during cooling will be reduced, and inclusions may partially or entirely retain the different $\delta^{18}O$ they had at the time of garnet growth. Under these circumstances, quartz inclusions in garnet may contain information about the evolution of the $\delta^{18}O$ of minerals in rocks along the prograde path of metamorphism. Accordingly, the absence or near absence of a statistically significant distinction between the $\delta^{18}O$ of quartz inclusions in garnet in samples 21-24C and Q2A and that of nearby matrix quartz grains alternatively could be explained by resetting of the $\delta^{18}O$ of quartz inclusions by oxygen isotope exchange with matrix grains along cracks in garnet following garnet growth. If so, there possibly could have been a change in $\delta^{18}O$ of quartz associated with the textural changes in samples 21-24C and Q2A that occurred in the matrix following garnet growth.

The absence of any correlation between the $\delta^{18}O$ of quartz inclusions in garnet in sample 21-25C (Fig. 10b) and whether the inclusion is connected or not to a visible crack could be explained in two ways. First, quartz inclusions that appear unconnected to a crack but with $\delta^{18}O$ statistically indistinguishable from that of nearby matrix quartz grains could be connected to a crack outside the plane of the thin section. Second, in cases where quartz inclusions are connected to a crack and the inclusion has $\delta^{18}O$ significantly lower than that of nearby matrix quartz grains, the crack could have formed after the rock cooled below the T at which oxygen diffusion in quartz had effectively ceased.

6.4. Outcrop- and regional-scale changes in oxygen isotope composition during regional metamorphism

It has been established for more than fifty years that the $\delta^{18}O$ of unaltered marine carbonate rocks is normally 10–15‰ higher than that of siliciclastic sediments (e.g., review by Taylor, 1967), and this mixture of sources is reflected in the $\delta^{18}O$ of calc-silicate marbles (Valley and O'Neil, 1984) and marls (Rumble et al., 1991). The weighted mean $\delta^{18}O$ of quartz in metamorphosed marls, psammites, and pelites in individual outcrops from the Gile Mountain Formation, eastern Vermont, however, differ by <0.5‰ (Figs. 1 and 16; Table 2). This study thus reveals a significant homogenization of $\delta^{18}O$ among layers of differing rock type (and hence differing protolith $\delta^{18}O$) at the outcrop scale during regional Barrovian metamorphism, at least in eastern Vermont. Layering is on a scale of decimeters (Ferry, 1994), and isotope transport must have been at the same or a larger spatial scale, probably by diffusion along wet grain boundaries (Bickle et al., 1997). The degree in homogeneity of $\delta^{18}O$ of quartz does not differ between lower grades of the biotite zone and higher grades of the kyanite zone. The observed homogenization of $\delta^{18}O$ of quartz during regional metamorphism at the outcrop scale (Fig. 16) closely parallels evidence for outcrop-scale homogenization of the CO_2 content of metamorphic fluid in eastern Vermont (Penniston-Dorland and Ferry, 2006; Ferry, 2007).

Although $\delta^{18}O$ of quartz is nearly uniform across different lithologies at the outcrop scale, there is a significant trend in decreasing $\delta^{18}O$ of quartz with increasing metamorphic grade in the Gile Mountain Formation, eastern
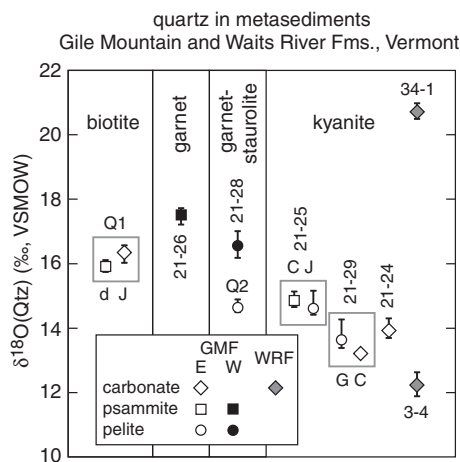

Fig. 16. Summary of the $\delta^{18}O$ of matrix quartz in regionally metamorphosed sedimentary rocks from eastern Vermont, organized by metamorphic grade and rock type. Symbols represent the weighted mean of the largest group of quartz analyses in a sample that are statistically indistinguishable. When larger than the size of a symbol, the vertical bar represents the range in all measured values. Numbers are sample localities (Table 2; see Fig. 1 for those in the Gile Mountain Formation). Boxes surround data from the same locality (letters correlate symbols for locations Q1, 21-25, and 21-29 to sample designations in Table 2). The $\delta^{18}O$ of quartz is nearly the same in different lithologies from the same sample locality. Ignoring locality 34-1, there is a regional decrease in the $\delta^{18}O$ of quartz of ~1–4‰ between the biotite and kyanite zones.

Vermont. The $\delta^{18}O$ of quartz in the biotite zone is ~16‰, while $\delta^{18}O$ of quartz is 13–15‰ in the kyanite zone. The $\delta^{18}O$ of quartz is consistently higher in the western exposure of the Gile Mountain Formation, Fig. 1, than in the eastern exposure, but a similar trend in decreasing $\delta^{18}O$ of quartz with increasing grade is also exhibited by samples 21-26E and 21-28A in the western exposure (Fig. 16). The difference in $\delta^{18}O$ of quartz between the biotite and kyanite zones (Fig. 16) is too large to be attributed to closed-system garnet-forming reactions during prograde metamorphism (Kohn, 1993). The trend in $\delta^{18}O$ of quartz illustrated in Fig. 16 has been observed elsewhere (e.g., Wickham and Taylor, 1985; Bowman et al., 2003), and is interpreted as increasing ^{18}O–^{16}O exchange between rocks and infiltrating low-$\delta^{18}O$ fluids with increasing grade of metamorphism. In the case of eastern Vermont, the interpretation is consistent with abundant petrologic and stable isotopic evidence for infiltration of metasedimentary rocks by chemically reactive fluids during regional metamorphism (Ferry, 1988, 1992, 1994; Barnett and Chamberlain, 1991; Stern et al., 1992; Wing and Ferry, 2007). Data for sample 3-4G from the Waits River Formation in eastern Vermont (Fig. 16) indicate a magmatic source for the low-$\delta^{18}O$ fluids, at least in some cases. The weighted mean $\delta^{18}O$ of quartz in sample 3-4G (12.2‰, Table 2), is the lowest of all analyzed quartz from Vermont, and the sample was collected from the diopside zone of a deep crustal contact aureole around a syn-metamorphic granite pluton that has a broad halo of lowered $\delta^{18}O$ (Ferry, 1992; Stern et al., 1992; Wing and Ferry, 2007). In the case of sample 3-4G, low-$\delta^{18}O$ fluids that caused lowering of $\delta^{18}O$ of the country rock seem to have been magmatic. Data for sample 34-1A, however, are a counterexample. Sample 34-1A also experienced infiltration-driven metamorphism and occurs in the diopside zone of a deep crustal contact aureole around another syn-metamorphic granite pluton (Ferry, 1992). The sample, however, contains quartz with the highest measured $\delta^{18}O$ in the entire study (weighted mean, 20.7‰, Table 2), close to the range of $\delta^{18}O$ of quartz that would be in equilibrium with unaltered marine carbonate rocks. Fluids in the second aureole appear to have caused little if any lowering of $\delta^{18}O$ in country rocks currently exposed around the pluton (Stern et al., 1992). The difference between the $\delta^{18}O$ of quartz in samples 3-4G and 34-1A could be explained if sample 3-4G occurred upstream from, and sample 34-1A occurred downstream from, the oxygen isotope alteration front in the two aureoles (Ferry and Rumble, 1997). Further work, however, would be required to evaluate this possibility. The rapid $\delta^{18}O$ analysis of minerals like quartz by ion microprobe opens additional opportunities to resolve questions like this one involving spatial patterns of the isotopic composition of metamorphic rocks and minerals on a regional scale.

6.5. Prospects for oxygen isotope thermometry in metamorphic rocks

Results of this study point to a great, but yet unrealized, potential for isotope thermometry using ion microprobe analysis. An example of the promise is exhibited by kyanite

and quartz in sample Gass that have weighted mean $\delta^{18}O$ values of $12.65 \pm 0.11‰$ and $15.62 \pm 0.07‰$ ($\pm 2SE$), respectively (Table 2). Using the calibration of quartz-kyanite oxygen isotope fractionation by Sharp (1995), the T recorded by the quartz-kyanite fractionation has an uncertainty of $\pm 18\,°C$. Of the 17 samples represented in Figs. 11 and 12, ten contain one or more minerals with $\delta^{18}O$ far from equilibrium with others in the same sample at the inferred T of mineral equilibrium. The significant departure from equilibrium may be either because some minerals failed to equilibrate with coexisting minerals at or near peak T during metamorphism (such as forsterite in sample KP1B and wollastonite in sample CL30O, Fig. 11) or because some minerals have $\delta^{18}O$ altered during cooling (such as calcite, K-feldspar, and plagioclase in samples 3-4G and 34-1A, Fig. 12d). In either case, besides adequate analytical precision, ion microprobe analysis provides a rapid and effective way to identify minerals in samples like these with $\delta^{18}O$ unsuitable for isotope thermometry (and to elucidate otherwise unrecognized metamorphic processes that may have caused such selective disequilibrium).

Before the promise for routine, precise oxygen isotope thermometry by ion microprobe can be fully realized, however, additional work is needed on three fronts. First, bias*(unknown) corrections for certain key mineral solid solutions need to be more completely calibrated, especially garnet (see Appendix A). Second, the T dependence of equilibrium isotope fractionation among key minerals pairs needs to be better determined. For example, the uncertainty in the value of A(quartz-garnet) in Table 5, $\pm 0.22‰$ (Valley et al., 2003), and the uncertainty in the value of the factor that relates A(quartz-garnet) to A(quartz-kyanite), ± 0.02 (Sharp, 1995), introduce an uncertainty in the T recorded by quartz-kyanite oxygen isotope fractionation in sample Gass of $\pm 45\,°C$, an uncertainty 2.5 times that introduced by the analytical uncertainty of the ion microprobe. Targets for further investigation include not only quartz-kyanite fractionation but also fractionations involving a range of garnet, diopside, olivine, and dolomite solid solutions. Third, rate constants for recrystallization and volume diffusion are poorly known for many minerals and need additional experimental study (Cole and Chakraborty, 2001). Improved measurements of the rate constants will allow better evaluation of the conditions and environments of metamorphism best suited to meaningful application of oxygen isotope thermometry.

ACKNOWLEDGMENTS

APPENDIX A

A.1. Data correcion

Correction of raw $\delta^{18}O$ values of unknowns followed procedures established at the Wisc-SIMS Laboratory (Ushikubo et al., 2012; Nakashima et al., 2013; Tenner et al., 2013). Following Tenner et al. (2013), corrections to raw measured values of $\delta^{18}O$ were made with two separate terms. One term, bias(WS) in the notation of Tenner et al. (2013), where WS refers to the working standard, corrects for fractionation of oxygen isotopes by the instrument during analysis of the unknowns. The computation of bias(WS) involves the raw $\delta^{18}O$ of the working standard measured during analysis of the unknowns [$\delta^{18}O$(WS,raw)] and the $\delta^{18}O$ of the working standard on the VSMOW scale [$\delta^{18}O$(WS,VSMOW)] as calibrated independently:

$$bias(\text{WS}) = \left[\frac{\delta^{18}O(\text{WS, raw}) + 1000}{\delta^{18}O(\text{WS, VSMOW}) + 1000} - 1 \right] 1000(‰).$$

(A.1)

The second term, bias*(unknown), corrects for the difference in chemical composition between each unknown mineral and the working standard (i. e., a correction for matrix effects). (The second term is not used if the unknown and the working standard are identical in chemical composition.) Computation of bias*(unknown) is based on measurements of (1) the raw $\delta^{18}O$ of a working standard, (2) the $\delta^{18}O$ of the working standard on the VSMOW scale, (3) the raw $\delta^{18}O$ of a standard that corrects for matrix effects (MS) [$\delta^{18}O$(MS,raw)], and the $\delta^{18}O$ of the standard used to correct for matrix effects on the VSMOW scale [$\delta^{18}O$(MS,VSMOW)]:

$$bias^*(unknown)$$
$$= \left\{ \frac{[\delta^{18}O(\text{MS, raw}) + 1000][\delta^{18}O(\text{WS, VSMOW}) + 1000]}{[\delta^{18}O(\text{MS, VSMOW}) + 1000][\delta^{18}O(\text{WS, raw}) + 1000]} - 1 \right\}$$
$$\times 1000‰.$$

(A.2)

The standards used to correct for matrix effects are chosen to match the chemical composition of the unknowns (Table A.1). Values of $\delta^{18}O$ of standards on the VSMOW scale were determined using laser fluorination (silicates) or acid digestion (carbonates) techniques at the University of Wisconsin. The total correction that links the raw $\delta^{18}O$ of an unknown mineral, bias(WS), and bias*(unknown) to the reported $\delta^{18}O$ of the unknown mineral on the VSMOW scale is:

$$bias = \left[\left(1 + \frac{bias^*(unknown)}{1000} \right) \left(1 + \frac{bias(\text{WS})}{1000} \right) - 1 \right] 1000‰; \quad (A.3)$$

$$\delta^{18}O(\text{unknown, VSMOW}) = \left[\frac{\delta^{18}O(\text{unknown, raw}) + 1000}{bias + 1000} - 1 \right] 1000‰.$$

(A.4)

Specifically, for the unknowns that are pure substances (kyanite, quartz, and wollastonite), bias*(unknown) was calibrated using a single mineral standard (09K3, UWQ1, and UWW-1, respectively, Table A.1). In principle, bias*(unknown) for forsterite, K-feldspar, and diopside

Table A.1
Oxygen isotope and relevant chemical data for standards.

Mineral	Standard name	$\delta^{18}O^a$ (‰, VSMOW)	X^b	Reference(s)[c]
Calcite[d]	UWC1	23.36	0.00	1
Calcite[d]	UWC3	12.49	0.02	2
Diopside	95AK-6	23.98	0.03	3
Diopside	92LEW-3	−0.84	0.41	4,5
Diopside	92LEW-9	−0.26	0.58	4,5
Diopside	92LEW-7	−0.78	0.66	4,5
Dolomite[d]	UW6220	22.72	0.50	1
Forsterite	San Carlos olivine	5.32	0.89	6
Garnet	PypDM	5.60	0.00	7
Garnet	SpsSE	5.40	0.00	7
Garnet	AlmSE	8.30	0.01	7
Garnet	Pp-1	6.30	0.02	5
Garnet	Sps-2	3.79	0.02	5
Garnet	Bal509	12.30	0.03	7
Garnet	Beta114	9.30	0.06	7
Garnet[d]	UWG2	5.80	0.14	8
Garnet	13-63-44	6.37	0.25	7
Garnet	R-53	5.33	0.61	7
Garnet	GrsSE	3.80	0.94	7
K-feldspar	FCS	7.06	0.75	9
K-feldspar	Gem28	13.15	0.93	9
Kyanite	09K3	6.84		10
Plagioclase	Amelia albite	10.8	0.00	11
Plagioclase	Ontario	14.27	0.13	11
Plagioclase	HAWK	6.72	0.22	11
Plagioclase	Tanzania	6.02	0.37	11
Plagioclase	Sierra Leone	6.28	0.60	11
Plagioclase	Sittam Pundi	6.19	0.90	11
Quartz[d]	UWQ1	12.33		12
Wollastonite	UWW-1	−0.04		5

[a] Determined by laser fluorination (silicates) or acid digestion (carbonates) techniques.
[b] Calcite and dolomite: $X^*_{Mg} = Mg/(Ca + Mg + Fe + Mn)$, diopside: $X_{Fe} = Fe/(Mg + Fe)$, forsterite: $X_{Mg} = Mg/(Mg + Fe)$, garnet: X_{gr} = mole fraction grossular component, K-feldspar: $X_K = K/(K + Na)$, plagioclase: X_{an} = mole fraction anorthite component.
[c] References: 1 = Bowman et al. (2009); 2 = Kozdon et al. (2009); 3 = Edwards and Valley (1998); 4 = Kohn and Valley (1998); 5 = this study; 6 = Kita et al. (2010); 7 = Page et al. (2010); 8 = Valley et al. (1995); 9 = Pollington (2013); 10 = Huberty (2010); 11 = Nakashima et al. (2013), their Table A3; 12 = Kelly et al. (2007).
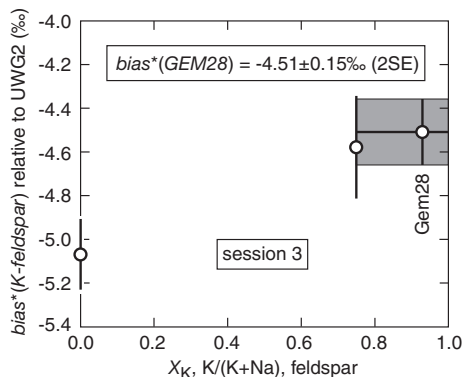[d] Working standard.

Fig. A.1. Measured *bias**(*K-feldspar*) during analytical session 3 of the two K-feldspar standards and of Amelia albite (Table A.1) with respect to working garnet standard UWG2, plotted against feldspar composition. Horizontal line is the value for standard Gem28, and the gray band and vertical black lines are ±2SE. There is no statistically significant variation in *bias**(*K-feldspar*) with composition in the range $X_K = 0.75$–1.00.
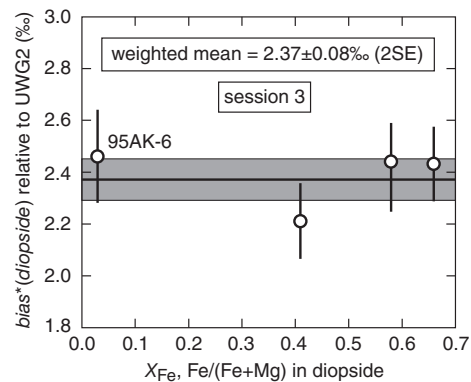

Fig. A.2. Measured *bias**(*diopside*) during analytical session 3 of the four diopside standards (Table A.1) with respect to working garnet standard UWG2, plotted against diopside composition. There is no statistically significant variation in *bias**(*diopside*) with composition in the range $X_{Fe} = 0.03$–0.66. Horizontal line is the weighted mean value for the four diopside standards. The vertical lines and the gray band are ±2SE for the individual measurements and for the weighted mean, respectively.
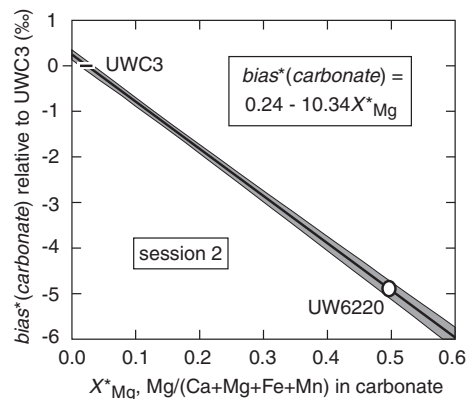
Fig. A.3. Measured *bias**(*carbonate*) with respect to working calcite standard UWC3 during analytical session 2 plotted against carbonate composition. Error bar and error ellipse correspond to ±0.01 uncertainties in X^*_{Mg} and (for UW6220) ±2SE in the measured *bias**(*carbonate*). The linear fit defines the dependence of *bias**(*carbonate*) on carbonate composition for calcite and dolomite, using UWC3 as the working standard and analysis during analytical session 2. Grey band is the 95% confidence interval in *bias**(*carbonate*), computed using Isoplot 3.00 (Ludwig, 2003).

Fig. A.5. Measured *bias**(*garnet*) of the eleven garnet standards (Table A.1) with respect to working garnet standard UWG2 during analytical session 2 plotted against garnet composition. When larger than the size of the symbol, the vertical line represents ±2SE in the measured value for that datum. The quadratic fit to the standards represented by filled circles defines the preferred dependence of *bias**(*garnet*) on garnet composition, using UWG2 as the working standard and analysis during analytical session 2. Values of *bias**(*garnet*) of the other five standards were omitted from the calibration because they have very Mg- or Mn-rich compositions unlike the analyzed unknowns. The gray band illustrates the range in X_{gr} measured for all analyzed garnets from regional metamorphic rocks of this study.
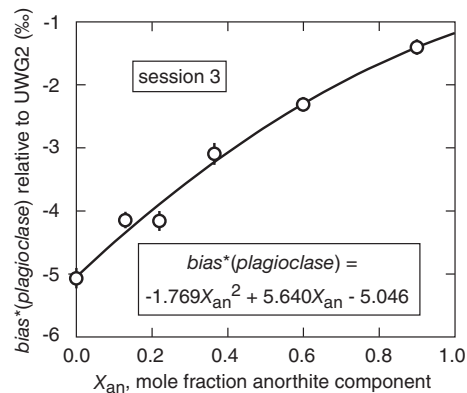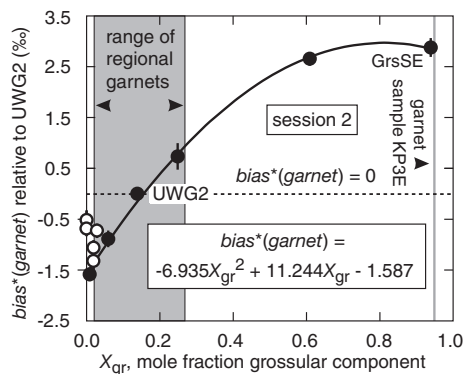

Fig. A.4. Measured *bias**(*plagioclase*) of the six plagioclase standards (Table A.1) with respect to working garnet standard UWG2 during analytical session 3 plotted against plagioclase composition. When larger than the size of the symbol, the vertical line represents ±2SE in *bias**(*plagioclase*) for that datum. The quadratic fit to all six standards defines the dependence of *bias**(*plagioclase*) on feldspar composition, using UWG2 as the working standard and analysis during analytical session 3.

depend on the composition of analyzed mineral solid solutions. Over the range of compositions of analyzed unknown forsterite ($X_{Mg} = 0.95–1.00$), K-feldspar ($X_K = 0.94–0.98$), and diopside ($X_{Fe} = 0.01–0.33$), however, there is no significant dependence of *bias**(*unknown*) on mineral composition (Kita et al., 2010; Figs. A.1 and A.2; Table A.1). Values of *bias**(*forsterite*) and *bias**(*K-feldspar*) were calibrated using a single mineral standard, San Carlos olivine

and Gem38, respectively (Table A.1, Fig. A.1). In one analytical session in which only diopside in a sample with $X_{Fe} = 0.00$ was analyzed, *bias**(*diopside*) was calibrated using a single mineral standard, 95AK-6, with $X_{Fe} = 0.03$ (Table A.1). In a second analytical session in which diopsides with $X_{Fe} = 0.03–0.34$ were analyzed, *bias**(*diopside*) was calibrated using the weighted mean value for all four diopside standards (Fig. A.2). Values of *bias**(*unknown*) for calcite, dolomite, plagioclase, and garnet, on the other hand, vary significantly over the range of mineral compositions of analyzed unknowns. The compositional dependence of *bias**(*carbonate*) was calibrated by a linear fit of X^*_{Mg} to *bias**(*dolomite*) (UW6220 standard) and *bias**(*calcite*) (UWC1 or UWC3 standards) (Table A.1); an example is illustrated in Fig. A.3. In detail, the relation between *bias**(*carbonate*) and X^*_{Mg} may not be linear (Valley and Kita, 2009, Figs. 2–10D), but this difference is not significant for unknown compositions close to endmember calcite or dolomite. The compositional dependence of *bias**(*plagioclase*) was calibrated by a quadratic fit of X_{an} to *bias**(*plagioclase*) measured for all six plagioclase standards (Table A.1, Fig. A.4). Following Page et al. (2010), the compositional dependence of *bias**(*garnet*) was calibrated by a quadratic fit of X_{gr} to *bias**(*garnet*) measured for six of the eleven garnet standards (Table A.1; filled circles in Fig. A.5). Values of *bias**(*garnet*) of the other five garnet standards were omitted from the fit because these standards have very Mg- and Mn-rich compositions unlike those of the analyzed unknown garnets of this study.

A.2. Error analysis

For a bias involving two $\delta^{18}O$ values, $\delta^{18}O(a)$ and $\delta^{18}O(b)$,

$$bias = \left[\frac{\delta^{18}O(a) + 1000}{\delta^{18}O(b) + 1000} - 1\right] 1000$$

$$= \left[\frac{\delta^{18}O(a) - \delta^{18}O(b)}{\delta^{18}O(b) + 1000}\right] 1000$$

$$\approx \delta^{18}O(a) - \delta^{18}O(b) \qquad (A.5)$$

(cf. Eq. (A.1)). Provided that $\delta^{18}O(b)$ is reasonably close to zero ($\leqslant 20\permil$), error in bias introduced by the approximation is small, $\leqslant 0.2\%$. In the approximation for a *bias* that involves more than two $\delta^{18}O$ values (e. g., Eq. (A.2)), *bias* is the difference between two or more differences in $\delta^{18}O$. For simplicity of calculation, therefore, the error analysis was based on the approximation that both *bias(*WS) and *bias**(*unknown*) are a series of additions and subtractions of $\delta^{18}O$ values. The uncertainty in *bias(*WS), *bias**(*unknown*), and *bias* were computed from estimates of the uncertainty in measured values of non-canceling $\delta^{18}O$ terms that were then appropriately added in quadrature.

The uncertainty in the raw $\delta^{18}O$ of an unknown mineral was estimated as the standard deviation (SD) of the eight bracketing values of the raw $\delta^{18}O$ of the working standard. The uncertainty in the raw $\delta^{18}O$ of all standards was estimated as one standard error of the mean (SE), calculated as the SD of all related measurements of the standard divided by the square root of the number of analyses. The uncertainty in $\delta^{18}O$ of all standards on the VSMOW scale was estimated as a $SE = 0.05\permil$ based on experience at the University of Wisconsin in analysis of silicates by laser fluorination techniques and of carbonates by acid digestion. For diopsides with $X_{Fe} = 0.03–0.34$, the uncertainty in *bias**(*diopside*) was estimated as the SE of measurements of *bias**(*diopside*) of the four diopside standards (Fig. A.2).

Uncertainties in the *bias**(*unknown*) of calcite, dolomite, plagioclase, and garnet contain an additional term for uncertainty introduced by the measurement of the cation composition of the minerals at the site of ion microprobe analysis (determined by electron microprobe analysis). This added uncertainty was estimated as $0.01b$, where b is the slope of the calibration line or curve in Figs. A.3–A.5 at the relevant composition, and 0.01 is the estimated 1SD uncertainty in X^*_{Mg}, X_{an}, and X_{gr}. The uncertainty in *bias**(*carbonate*) was estimated as one quarter of the 95% confidence interval in the linear fit of *bias**(*carbonate*) against X^*_{Mg} (Fig. A.3), added in quadrature with $0.01b$. The uncertainty in *bias**(*plagioclase*) was estimated as $0.5\sqrt{(\sum R_i^2/6)}$, added in quadrature with $0.01b$ (R_i is the deviation in measured *bias**(*plagioclase*) of each of the $i = 6$ plagioclase standards from the quadratic fit of *bias**(*plagioclase*) against X_{an} in Fig. A.4). Garnet in contact metamorphosed sample KP3E has $X_{gr} = 0.95$ almost identical to the X_{gr} of garnet standard GrsSE (Table A.1, Fig. A.5). The uncertainty in *bias**(*garnet*) for sample KP3E therefore was taken as the uncertainty in the measured value of *bias**(*GrsSE*), added in quadrature with

$0.01b$. The effects of variability of components other than grossular on *bias**(*garnet*) are not yet well determined. Values of *bias**(*garnet*) for garnet standards with $X_{gr} < 0.06$ suggest that corrections for components other than grossular could be up to $\sim 1\permil$. The uncertainty in *bias**(*garnet*) for compositions of the analyzed garnets in regional metamorphic rocks (gray band, Fig. A.5), expressed as a SD, therefore, were taken somewhat arbitrarily as $0.25\permil$ added in quadrature with $0.01b$.

Values of SD(1) in Table 2 and the text are based exclusively on the eight measurements of the raw $\delta^{18}O$ of the working standard that bracket each group of unknown analyses. The uncertainty in $\delta^{18}O$(unknown,VSMOW), defined by the of the combination of the uncertainties in raw $\delta^{18}O$ of an unknown, in *bias(*WS), and in *bias**(*unknown*) in Eqs. (A.3) and (A.4) and expressed as one standard deviation, corresponds to SD(2) in Table 2 and the text. The preferred estimate of the uncertainty in the reported value of $\delta^{18}O$ of an unknown on the VSMOW scale therefore is SD(2).

APPENDIX B. SUPPLEMENTARY DATA

Supplementary data associated with this article can be found, in the online version, at http://dx.doi.org/10.1016/j.gca.2014.08.021.

REFERENCES

Armstrong J. T. (1995) CITZAF: a package of correction programs for the quantitative correction of microbeam X-ray analysis of thick polished materials, thin films, and particles. *Microbeam Anal.* **4**, 177–200.

Barnett D. E. and Chamberlain C. P. (1991) Relative scales of thermal- and fluid infiltration-driven metamorphism in fold nappes, New England, USA. *Am. Mineral.* **76**, 713–727.

Bickle M. J., Chapman H. J., Ferry J. M., Rumble, III, D. and Fallick A. E. (1997) Fluid flow and diffusion in the Waterville limestone, south-central Maine: constraints from strontium, oxygen and carbon isotope profiles. *J. Petrol.* **38**, 1489–1512.

Bowman J. R., Valley J. W. and Kita N. T. (2009) Mechanisms of oxygen isotopic exchange and isotopic evolution of $^{18}O/^{16}O$-depleted periclase zone marbles in the Alta aureole, Utah: insights from ion microprobe analysis of calcite. *Contrib. Mineral. Petrol.* **157**, 77–93.

Bowman J. R., Sisson V. B., Valley J. W. and Pavlis T. L. (2003) Oxygen isotope constraints on fluid infiltration associated with high temperature – low pressure metamorphism (Chugach metamorphic complex) within the Eocene southern Alaska fore-arc. *Geol. Soc. Am. Spec. Pap.* **371**, 237–253.

Chiba H., Chacko T., Clayton R. N. and Goldsmith J. R. (1989) Oxygen isotope fractionations involving diopside, forsterite, magnetite, and calcite. *Geochim. Cosmochim. Acta* **53**, 2985–2995.

Clayton R. N., Goldsmith J. R. and Mayeda T. K. (1989) Oxygen isotope fractionation in quartz, albite, anorthite, and calcite. *Geochim. Cosmochim. Acta* **53**, 725–733.

Cole D. R. and Chakraborty S. (2001) Rates and mechanisms of isotopic exchange. In *Stable Isotope Geochemistry*, vol. 43 (eds. J. W. Valley and D. R. Cole). *Rev. Mineral. Geochem.* pp. 83–223.

Cook S. J., Bowman J. R. and Forster C. B. (1997) Contact metamorphism surrounding the Alta stock: finite element simulation of heat- and $^{18}O/^{16}O$ mass-transport during prograde metamorphism. *Am. J. Sci.* **297**, 1–55.

Crank J. (1975) *The Mathematics of Diffusion*. Oxford University Press, Oxford.

Davis S. R. and Ferry J. M. (1993) Fluid infiltration during contact metamorphism of interbedded marble and calc-silicate hornfels, Twin Lakes area, central Sierra Nevada, California. *J. Metamorph. Geol.* **11**, 71–88.

Doll, C. G., Cady, W. M., Thompson, Jr., J. B. and Billings, M. P. (eds.) (1961) *Centennial Geologic Map of Vermont*. Vermont Geologic Survey, Montpelier.

Edwards K. J. and Valley J. W. (1998) Oxygen isotope diffusion and zoning in diopside: the importance of water fugacity during cooling. *Geochim. Cosmochim. Acta* **62**, 2265–2277.

Eiler J. M., Baumgartner L. P. and Valley J. W. (1992) Intercrystalline stable isotope diffusion: a fast grain boundary model. *Contrib. Mineral. Petrol.* **112**, 543–557.

Eiler J. M., Valley J. W. and Baumgartner L. P. (1993) A new look at stable isotope thermometry. *Geochim. Cosmochim. Acta* **57**, 2571–2583.

Ferry J. M. (1988) Infiltration-driven metamorphism in northern New England, USA. *J. Petrol.* **29**, 1121–1159.

Ferry J. M. (1992) Regional metamorphism of the Waits River Formation, eastern Vermont: delineation of a new type of giant metamorphic hydrothermal system. *J. Petrol.* **33**, 45–94.

Ferry J. M. (1994) Overview of the petrologic record of fluid flow during regional metamorphism in northern New England. *Am. J. Sci.* **294**, 905–988.

Ferry J. M. (1996a) Three novel isograds in metamorphosed siliceous dolomites from the Ballachulish aureole, Scotland. *Am. Mineral.* **81**, 485–494.

Ferry J. M. (1996b) Prograde and retrograde fluid flow during contact metamorphism of siliceous carbonate rocks from the Ballachulish aureole, Scotland. *Contrib. Mineral. Petrol.* **124**, 235–254.

Ferry J. M. (2001) Calcite inclusions in forsterite. *Am. Mineral.* **86**, 773–779.

Ferry J. M. (2007) The role of volatile transport by diffusion and dispersion in driving biotite-forming reactions during regional metamorphism of the Gile Mountain Formation, Vermont. *Am. Mineral.* **92**, 1288–1302.

Ferry J. M. and Rumble, III, D. (1997) Formation and destruction of periclase by fluid flow in two contact aureoles. *Contrib. Mineral. Petrol.* **128**, 313–334.

Ferry J. M., Wing B. A. and Rumble, III, D. (2001) Formation of wollastonite by chemically reactive fluid flow during contact metamorphism, Mt. Morrison pendant, Sierra Nevada, California, USA. *J. Petrol.* **42**, 1705–1728.

Ferry J. M., Ushikubo T. and Valley J. W. (2011) Formation of forsterite by silicification of dolomite during contact metamorphism. *J. Petrol.* **52**, 1619–1640.

Ferry J. M., Rumble, III, D., Wing B. A. and Penniston-Dorland S. C. (2005) A new interpretation of centimetre-scale variations in the progress of infiltration-driven metamorphic reactions: case study of carbonated metaperidotite, Val d'Efra, Central Alps, Switzerland. *J. Petrol.* **46**, 1725–1746.

Ferry J. M., Ushikubo T., Kita N. T. and Valley J. W. (2010) Assessment of grain-scale homogeneity of carbon and oxygen isotope compositions of minerals in carbonate-bearing metamorphic rocks by ion microprobe. *Geochim. Cosmochim. Acta* **74**, 6517–6540.

Fraser G. L., Pattison D. R. M. and Heaman L. M. (2004) Age of the Ballachulish and Glencoe Igneous Complexes (Scottish Highlands), and paragenesis of zircon, monazite and baddeleyite in the Ballachulish Aureole. *J. Geol. Soc. Lond.* **161**, 447–462.

Giletti B. J. and Yund R. A. (1984) Oxygen diffusion in quartz. *J. Geophys. Res.* **89**, 4039–4046.

Gordon S. M., Luffi P., Hacker B., Valley J., Spicuzza M., Kozdon R., Kelemen P., Ratshbacher L. and Minaev V. (2012) The thermal structure of continental crust in active orogens: insight from Miocene eclogite and granulite xenoliths of the Pamir Mountains. *J. Metamorph. Geol.* **30**, 413–434.

Holland T. J. B. and Powell R. (1990) An enlarged and updated internally consistent thermodynamic dataset with uncertainties and correlations: the system K_2O-Na_2O-CaO-MgO-MnO-FeO-Fe_2O_3-Al_2O_3-TiO_2-SiO_2-C-H_2O-O_2. *J. Metamorph. Geol.* **8**, 89–124.

Huberty J. M. (2010) Crystal orientation effects for analysis of $\delta^{18}O$ in magnetite and hematite by SIMS. M.S. thesis, Univ. of Wisconsin, Madison.

Huberty J. M., Kita N. T., Kozdon R., Heck P. R., Fournelle J. H., Spicuzza M. J., Xu H. and Valley J. W. (2010) Crystal orientation effects in $\delta^{18}O$ for magnetite and hematite by SIMS. *Chem. Geol.* **276**, 269–283.

Javoy M., Fourcade S. and Allegre C. J. (1970) Graphical method for examination of $^{18}O/^{16}O$ fractionations in silicate rocks. *Earth Planet. Sci. Lett.* **10**, 12–16.

Kelly J. L., Fu B., Kita N. T. and Valley J. W. (2007) Optically continuous silcrete quartz cements of the St. Peter Sandstone: high precision oxygen isotope analysis by ion microprobe. *Geochim. Cosmochim. Acta* **71**, 3812–3832.

Keiffer S. (1982) Thermodynamics and lattice vibrations of minerals. 5. applications to phase equilibria, isotopic fractionation, and high-pressure thermodynamic properties. *Rev. Geophys. Space Phys.* **20**, 827–849.

Kita N. T., Ushikubo T., Fu B. and Valley J. W. (2009) High precision SIMS oxygen isotope analyses and the effect of sample topography. *Chem. Geol.* **264**, 43–57.

Kita N. T., Nagahara H., Tachibana S., Tomomura S., Spicuzza M. J., Fournelle J. H. and Valley J. W. (2010) High precision SIMS oxygen three isotope study of chondrules in LL3 chondrites: role of ambient gas during chondrule formation. *Geochim. Cosmochim. Acta* **74**, 6610–6635.

Kohn M. J. (1993) Modeling of prograde mineral $\delta^{18}O$ changes in metamorphic systems. *Contrib. Mineral. Petrol.* **113**, 249–261.

Kohn M. J. and Valley J. W. (1998) Effects of cation substitutions in garnet and pyroxene on equilibrium oxygen isotope fractionations. *J. Metamorph. Geol.* **16**, 625–639.

Kohn M. J., Valley J. W., Elsenheimer D. and Spicuzza M. (1993) Oxygen isotope zoning in garnet and staurolite: evidence for closed system mineral growth during regional metamorphism. *Am. Mineral.* **78**, 988–1001.

Kozdon R., Ushikubo T., Kita N. T., Spicuzza M. and Valley J. W. (2009) Intratest oxygen isotope variability in planktonic foraminifera: new insights from in situ measurements by ion microprobe. *Chem. Geol.* **258**, 327–337.

Lackey J. S. and Valley J. W. (2004) Complex patterns of fluid flow during wollastonite formation in calcareous sandstones at Laurel Mountain, Mt. Morrison pendant, California. *Geol. Soc. Am. Bull.* **116**, 76–93.

Ludwig K. R. (2003) *ISOPLOT 3.0, A geochronological toolkit for Microsoft Excel*. Berkeley Geochronology Center, Berkeley.

Lyons J. B. (1955) Geology of the Hanover quadrangle, New Hampshire-Vermont. *Geol. Soc. Am. Bull.* **66**, 105–146.

Mahon K. I. (1996) The new "York" regression: application of an improved statistical method to geochemistry. *Inter. Geol. Rev.* **38**, 293–303.

Martin L. A. J., Ballèvre M., Boulvais P., Halfpenny A., Vanderhaeghe O., Duchêne S. and Deloule E. (2011) Garnet re-equilibration by coupled dissolution-reprecipitation: evidence from textural, major element and oxygen isotope zoning of 'cloudy' garnet. *J. Metamorph. Geol.* **29**, 213–231.

Martin L. A. J., Rubatto D., Crépisson C., Hermann J., Putlitz B. and Vitale-Brovarone A. (2014) Garnet oxygen analysis by SHRIMP-SI: matrix corrections and application to high-

pressure metasomatic rocks from Alpine Corsica. *Chem. Geol.* **374–375**, 25–36.

Masch L. and Heuss-Aßbichler S. (1991) Decarbonation reactions in siliceous dolomites and impure limestones. In *Equilibrium and Kinetics in Contact Metamorphism. The Ballachulish Igneous Complex and its Aureole* (eds. G. Voll, J. Töpel, D. R. M. Pattison and F. Seifert). Springer-Verlag, Berlin, pp. 211–227.

Matthews A., Goldsmith J. R. and Clayton R. N. (1983) Oxygen isotope fractionations involving pyroxenes: the calibration of mineral-pair geothermometers. *Geochim. Cosmochim. Acta* **47**, 631–644.

Müller T., Baumgartner L. P., Foster, Jr., C. T. and Vennemann T. W. (2004) Metastable prograde mineral reactions in contact aureoles. *Geology* **32**, 821–824.

Nabelek P. I., Hofmeister A. M. and Whittington A. G. (2012) The influence of temperature-dependent thermal diffusivity on the conductive cooling rates of plutons and temperature-time paths in contact aureoles. *Earth Planet. Sci. Lett.* **317–318**, 157–164.

Nakashima D., Kita N. T., Ushikubo T., Noguchi T., Nakamura T. and Valley J. W. (2013) Oxygen three-isotope ratios of silicate particles returned from asteroid Itokawa by the Hayabusa spacecraft: a strong link with equilibrated LL chondrites. *Earth Planet. Sci. Lett.* **379**, 127–136.

Page F. Z., Kita N. T. and Valley J. W. (2010) Ion microprobe analysis of oxygen isotopes in garnets of complex chemistry. *Chem. Geol.* **270**, 9–19.

Page F. Z., Essene E. J., Mukasa S. B. and Valley J. W. (2014) A garnet-zircon oxygen isotope record of subduction and exhumation fluids from the Franciscan Complex, California. *J. Petrol.* **55**, 103–131.

Penniston-Dorland S. C. and Ferry J. M. (2006) Development of spatial variations in reaction progress during regional metamorphism of micaceous carbonate rocks, northern New England. *Am. J. Sci.* **306**, 475–524.

Pollington A. D. (2013) Stable isotope signatures of diagenesis: natural and experimental studies. Ph.D. thesis, Univ. of Wisconsin, Madison.

Putlitz B., Valley J. W., Matthews A. and Katzir Y. (2002) Oxygen isotope thermometry of quartz-Al_2SiO_5 veins in high-grade metamorphic rocks on Naxos Island (Greece). *Contrib. Mineral. Petrol.* **143**, 350–359.

Raimondo T., Clark C., Hand M., Cliff J. and Harris C. (2012) High-resolution geochemical record of fluid-rock interaction in a mid-crustal shear zone: a comparative study of major element and oxygen isotope transport in garnet. *J. Metamorph. Geol.* **30**, 255–280.

Ratcliffe N. M., Aleinikoff J. N., Armstrong T. R., Walsh G. J. and Hames W. E. (2001) Intrusive relations and isotopic ages of Devonian granites in southern and central Vermont: evidence for a prolonged Acadian Orogeny and partitioning of compressional strain. *Geol. Soc. Am. Prog. Abs.* **33**, 981.

Ridley J. and Thompson A. B. (1986) The role of mineral kinetics in the development of metamorphic microtextures. In *Fluid-Rock Interactions during Metamorphism* (eds. J. V. Walther and B. J. Wood). Springer-Verlag, New York, pp. 154–193.

Roselle G. T., Baumgartner L. P. and Chapman J. A. (1997) Nucleation-dominated crystallization of forsterite in the Ubehebe Peak contact aureole, California. *Geology* **25**, 823–826.

Rosenbaum J. M. and Mattey D. P. (1995) Equilibrium garnet-calcite oxygen isotope fractionation. *Geochim. Cosmochim. Acta* **59**, 2839–2842.

Rubatto D., Hermann J., Berger A. and Engi M. (2009) Protracted fluid-induced melting during Barrovian metamorphism in the Central Alps. *Contrib. Mineral. Petrol.* **158**, 703–722.

Rumble D., III (1982) Stable isotope fractionation during metamorphic devolatilization reactions. In *Characterization of Metamorphism through Mineral Equilibria* (ed. J. M. Ferry), *Rev. Mineral.* **10**, pp. 327–353.

Rumble, III, D., Oliver N. H. S., Ferry J. M. and Hoering T. C. (1991) Carbon and oxygen isotope geochemistry of chlorite-zone rocks of the Waterville limestone, Maine, USA. *Am. Mineral.* **76**, 857–866.

Schertl H.-P., Neuser R. D., Sobolev N. V. and Shatsky V. S. (2004) UHP-metamorphic rocks from Dora Maira/Western Alps and Kokchetav/Kazakhstan: new insights using cathodoluminescence petrography. *Eur. J. Mineral.* **16**, 49–57.

Sharp Z. D. (1995) Oxygen isotope geochemistry of the Al_2SiO_5 polymorphs. *Am. J. Sci.* **295**, 1058–1071.

Stern L. A., Chamberlain C. P., Barnett D. E. and Ferry J. M. (1992) Stable isotope evidence for regional-scale fluid migration in a Barrovian metamorphic terrane, Vermont, USA. *Contrib. Mineral. Petrol.* **112**, 475–489.

Taylor, Jr., H. P. (1967) The oxygen isotope geochemistry of hydrothermal mineral deposits. In *Geochemistry of Hydrothermal Ore Deposits* (ed. H. L. Barnes). Holt, Rinehart, and Winston, New York, pp. 19–63.

Tenner T. J., Ushikubo T., Kurahashi E., Kita N. T. and Nagahara H. (2013) Oxygen isotope systematics of chondrule phenocrysts from the CO3.0 chondrite Yamato 82120: evidence for two distinct oxygen isotope reservoirs. *Geochim. Cosmochim. Acta* **102**, 226–245.

Tennie A., Hoffbauer R. and Hoernes S. (1998) The oxygen isotope fractionation behaviour of kyanite in experiment and nature. *Contrib. Mineral. Petrol.* **133**, 346–355.

Ushikubo T., Kimura M., Kita N. T. and Valley J. W. (2012) Primordial oxygen isotope reservoirs of the solar nebula recorded in chondrules in Acfer 094 carbonaceous chondrite. *Geochim. Cosmochim. Acta* **90**, 242–264.

Valley J.W. (2001) Stable isotope thermometry at high temperatures: In *Stable Isotope Geochemistry*, vol. 43 (eds. J. W. Valley and D. R. Cole). *Rev. Mineral. Geochem.* pp. 365–414.

Valley J. W. and O'Neil J. R. (1984) Fluid heterogeneity during granulite facies metamorphism in the Adirondacks: stable isotope evidence. *Contrib. Mineral. Petrol.* **85**, 158–173.

Valley J. W. and Kita N. T. (2009) In situ oxygen isotope geochemistry by ion microprobe. In *Secondary Ion Mass Spectrometry in the Earth Sciences* (ed. M. Fayek). *Mineral. Assoc. Canada Short Course* **41**, pp. 19–63.

Valley J. W., Bindeman I. N. and Peck W. H. (2003) Empirical calibration of oxygen isotope fractionation in zircon. *Geochim. Cosmochim. Acta* **67**, 3257–3266.

Valley J. W., Kitchen N., Kohn M. J., Niendorf C. R. and Spicuzza M. J. (1995) UWG-2, a garnet standard for oxygen isotope ratios: strategies for high precision and accuracy with laser heating. *Geochim. Cosmochim. Acta* **59**, 5223–5231.

Vance D. and Holland T. (1993) A detailed isotopic and petrological study of a single garnet from the Gassetts Schist, Vermont. *Contrib. Mineral. Petrol.* **114**, 101–118.

Wickham S. M. and Taylor, Jr., H. P. (1985) Stable isotopic evidence for large-scale seawater infiltration in a regional metamorphic terrane – the Trois Seigneurs massif, Pyrenees, France. *Contrib. Mineral. Petrol.* **91**, 122–137.

Wing B. A. and Ferry J. M. (2007) Magnitude and geometry of reactive fluid flow from direct inversion of spatial patterns of geochemical alteration. *Am. J. Sci.* **307**, 793–832.

Wing B. A., Ferry J. M. and Harrison T. M. (2003) Prograde destruction and formation of monazite and allanite during contact and regional metamorphism of pelites: petrology and geochronology. *Contrib. Mineral. Petrol.* **145**, 228–250.

Associate editor: Bjorn Jamtveit